VYSOKÉ UČENÍ TECHNICKÉ V BRNĚ
BRNO UNIVERSITY OF TECHNOLOGY

FAKULTA ELEKTROTECHNIKY A KOMUNIKAČNÍCH TECHNOLOGIÍ
FACULTY OF ELECTRICAL ENGINEERING AND COMMUNICATION

ÚSTAV RADIOELEKTRONIKY
DEPARTMENT OF RADIO ELECTRONICS

ŠIROKOPÁSMOVÁ NÍZKOPROFILOVÁ KRUHOVĚ POLARIZOVANÁ ANTÉNNÍ ŘADA
WIDEBAND LOW-PROFILE CIRCULARLY POLARIZED ANTENNA ARRAY

BAKALÁŘSKÁ PRÁCE
BACHELOR'S THESIS

AUTOR PRÁCE — Jhony Cristian Benites Ayala
AUTHOR

VEDOUCÍ PRÁCE — prof. Dr. Ing. Zbyněk Raida
SUPERVISOR

BRNO 2019

VYSOKÉ UČENÍ TECHNICKÉ V BRNĚ
FAKULTA ELEKTROTECHNIKY A KOMUNIKAČNÍCH TECHNOLOGIÍ

Bakalářská práce

bakalářský studijní obor **Elektronika a sdělovací technika**
Ústav radioelektroniky

Student: Jhony Cristian Benites Ayala ***ID:*** 164714
Ročník: 3 ***Akademický rok:*** 2018/19

NÁZEV TÉMATU:

Širokopásmová nízkoprofilová kruhově polarizovaná anténní řada

POKYNY PRO VYPRACOVÁNÍ:

Seznamte se s principem činnosti širokopásmové kruhově polarizované anténní řady popsané v [1]. Korektnost publikovaných parametrů ověřte podrobným porovnáním impedančních, směrových a polarizačních charakteristik s počítačovou simulací v programu CST Microwave Studio.

Anténní řadu přepočítejte z původního substrátu Taconic TLX (relativní permitivita 2,55, výška 3 mm) na vybraný dostupný substrát ARLON. Anténu optimalizujte z hlediska impedančního přizpůsobení, osového poměru a směrových charakteristik v pracovním pásmu od 5,5 do 7,0 GHz. Optimalizovanou anténu vyrobte a experimentálně ověřte její vlastnosti.

DOPORUČENÁ LITERATURA:

[1] HENGFEI XU; JIANYI ZHOU; QI WU; ZHIQIANG YU; WEI HONG; Wideband low-profile SIW cavity-backed circularly polarized antenna with high-gain and conical-beam radiation. IEEE Transactions on Antennas and Propagation, 2018, vol. 66, no. 3, p. 1179-1188.

[2] BALANIS, C. A.; Antenna Theory: Analysis and Design, 3 Edition, Hoboken: J. Wiley & Sons, 2005, ISBN: 0-471-66782-X.

Termín zadání: 4.2.2019 ***Termín odevzdání:*** 23.5.2019

Vedoucí práce: prof. Dr. Ing. Zbyněk Raida
Konzultant:

prof. Ing. Tomáš Kratochvíl, Ph.D.
předseda oborové rady

ABSTRACT

This bachelor's thesis is focused on the study of a novel type of wideband low-profile circular array antenna with circular polarization and high gain. The aim of this thesis is to design, optimize and implement the proposed antenna for a 5.5 - 7 GHz frequency band. The thesis deals with theoretical fundamentals in order to subsequently present the concept of the antenna. Furthermore, it describes its design and implementation stages. The antenna was designed in the full-wave program CST Microwave Studio and fabricated on dielectric substrate. Both simulated and measured property results are evaluated in the conclusion.

KEYWORDS

Circular array antenna, wideband antenna, substrate integrated waveguide, circular polarization, low profile, high gain, CST Microwave Studio.

BENITES AYALA, Jhony Cristian. *Wideband low-profile circularly polarized antenna array*. Brno: Brno University of Technology, Faculty of Electrical Engineering and Communication, Department of Radio Electronics, 2019. pp. 79. Bachelor's thesis. Supervisor: prof. Dr. Ing. Zbyněk Raida.

DECLARATION

I declare that I have worked on this bachelor's thesis on the topic "Wideband low-profile circularly polarized antenna array" independently under the guidance of my thesis supervisor, using only the primary and secondary sources cited in the bibliography at the end of the work.

I further declare that, as the author of this bachelor's thesis, I did not infringe the copyrights of third parties, in particular, I did not intervene in the personal and property copyright of others, and I am fully aware of the consequences of violation of § 11 et seq Law no. 121/2000 Coll., on copyright, rights related to copyright and amending some laws (Copyright Act), as amended, including possible criminal consequences arising from the provisions of Part II, Title VI. Part 4 of the Penal Code no. 40/2009.

Brno, 23rd May 2019 .....

(Author's signature)

ACKNOWLEDGEMENT

I would like to express my sincere gratitude to my supervisor Prof. Dr. Ing. Zbyněk Raida for his continuous support for this bachelor's thesis, as well as for his patience, motivation, and valuable advice.

Faculty of Electrical Engineering
and Communication

Brno University of Technology
Technicka 12, CZ-61600 Brno, Czech Republic

http://www.six.feec.vutbr.cz

Experimentální část této bakalářské práce byla realizována na výzkumné infrastruktuře vybudované v rámci projektu CZ.1.05/2.1.00/03.0072
Centrum senzorických, informačních a komunikačních systémů (SIX)
operačního programu Výzkum a vývoj pro inovace.

TABLE OF CONTENTS

INDEX OF ILLUSTRATIONS

INDEX OF TABLES

INTRODUCTION

During the last years, circularly polarized (CP) antennas have been widely used in several contemporary wireless communication systems, such as satellite communication, vehicles communication, radar, WLAN (Wireless Local Area Network), WiMAX (Worldwide Interoperability for Microwave Access), GPS (Global Positioning System), and other wireless systems, because of their suitable characteristics, good performance and versatile orientation of the transmitter-receiver.

The main objective of this bachelor's thesis is to study, design, optimize and fabricate a novel type of wideband low-profile circular array antenna with circular polarization and high gain, proposed in the primary literature of the present work.

This thesis is divided in two principal parts. In the first part, fundamentals about microstrip and slot antennas, their essential characteristics and parameters, feeding, substrate integrated waveguide cavity resonator and planar circular array are covered to introduce the reader to the design concept and the operating mechanism of the investigated antenna.

The second part presents the design and realization approach in the present work for creating the proposed antenna. This practical part is divided in 7 sections. The first Section 2.1 focuses on the method, steps and considerations performed in the full-wave program CST Microwave Studio for the numerical design and optimization of the antenna. Sections 2.2 - 2.4 are focused on simulations for three numerical designs with different dielectric substrates – Taconic TLX, Arlon CuClad 217, and Rogers 5870. Furthermore, the optimization procedure of the antenna for the last two substrates is explained in detail. Sections 2.5 and 2.6 describe the fabrication and experimental verification of simulated results of the antenna, respectively. Finally, Section 2.7 makes a comparison of performance of the present work with other studies cited in the literature which focused on similar antenna concepts.

1 THEORETICAL PART

1.1 About microstrip planar antennas

In recent years, microstrip planar antennas have been popularly proposed and developed due to their suitable characteristics for wireless applications. Therefore, they are significantly compatible with embedded antennas in wireless devices, such as mobile phones, personal digital assistant (PDA) devices, wireless routers, wireless computer peripherals, remote controls, global positioning system (GPS) devices, and so on.

Microstrip planar antennas operates at the wideband frequency range from 100 MHz to 100 GHz, outside the range of conventional antennas. Let us address some advantages and disadvantages in comparison with other common types of microwave antennas [3].

1.1.1 Advantages

- Low profile – low volume and light weight.
- Support of dual polarization – linear as well as circular polarization are possible with simple feed.
- Support of multiple frequency bands – dual as well as triple.
- Ease of fabrication on a planar surface and low implementation cost – printed antenna similarly to printed circuit board (PCB).
- Great variety of patch shapes as radiators for different applications – square, rectangular, circular, elliptical, triangular, etc., which are easily etched.
- Ease of adaptation with microwave integrated circuit (MIC).

1.1.2 Disadvantages

- Narrow bandwidth – typically 1-5%, effected by the permittivity and thickness of substrate.
- Low efficiency – due to dielectric and conductor loss.
- Low power handling capability – nearly 100 W.
- Low gain – nearly 6 dB.
- Inherent type of radiation – most microstrip antennas radiate in the half-space above the ground plane, they also radiate from feeds and other junction points.
- High antenna quality factor (Q) – causes a narrow bandwidth and low efficiency.

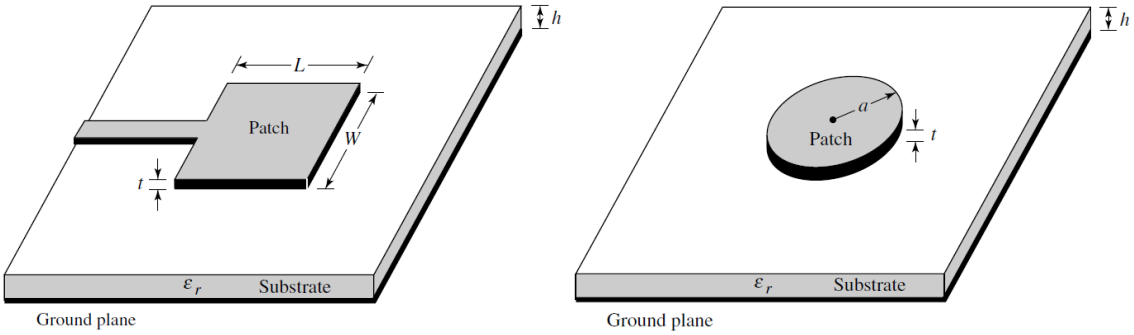

Figure 1.1 Most typical microstrip planar antennas – a) Rectangular, b) Circular [1].

1.1.3 Applications

As previously mentioned, microstrip planar antennas are very popular because of their good performance, compact design, easy and low-cost fabrication for modern uses. They are becoming very commercial in fields such as satellite, medical and military. Some of their principal applications are [4]:

- Satellite communication such as direct broadcasting satellite (DBS) services.
- Satellite navigation receivers.
- Doppler and other radar systems.
- Missiles and telemetry.
- Command and control systems.
- Remote sensing and environmental instrumentation.
- Mobile radio.
- Antennas array, integrated antennas, feed elements in complex antennas.
- Security systems such as intruder alarms.
- Biomedical radiators.

1.1.4 Shapes of antenna radiator

Microstrip planar antennas are designed with many different shapes and dimensions depending on the purpose of their application. It was found out that some radiator shapes (also called “patches”) have very low *Q* and wider bandwidth in comparison with other shapes. Shapes such as annular ring, circular, quarter-wavelength rectangular belong to this group [4]. Bandwidth of annular and rectangular shapes are presented in Table 1.1.

As can be observed, the bandwidth of rectangular shapes increases by increasing their width (*W*) and additionally, the annular ring shape presents the widest bandwidth among these listed radiator shapes.

Table 1.1 Summary of radiator shapes and their bandwidth for ε_r=2.32, h =1.59 cm, f =2 GHz [4].

Radiator shape	Dimensions [cm]	Bandwidth [%]
Narrow rectangle	L=4.924, W=2	0.7
Wide rectangle	L=4.79, W=7.2	1.6
Square	L=W=4.82	1.3
Circle	a=2.78	1.3
Annular ring	a=4.45, b=8.9	3.8

In Figure 1.2 basic shapes which are used typically as radiators are shown. The radiator shape influences the current distribution in the antenna and consequently, the radiation patterns as well. Another parameter that affects the bandwidth is the radiator material. A suitable conductive material should be chosen for this purpose. For design of microstrip patch antennas copper is commonly used.

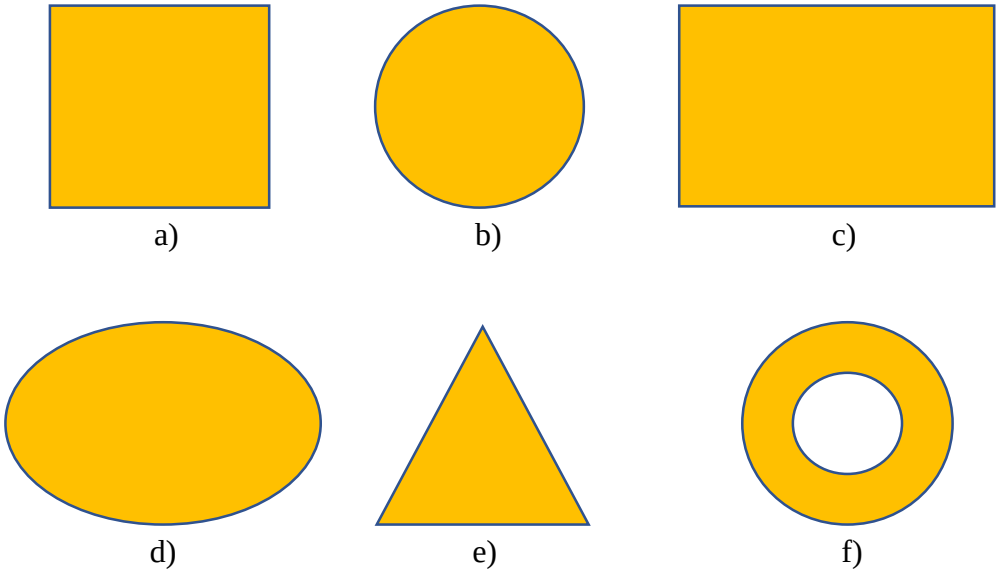

Figure 1.2 Commonly used microstrip patch antenna shapes – a) Square, b) Circular, c) Rectangular, d) Elliptical, e) Triangular, f) Annular ring [4].

1.1.5 Slot antennas

Slot antennas are used typically at frequencies between 300 MHz and 24 GHz. The slot antenna is widely popular because they can be cut out of whatever surface they are to be mounted on, and have radiation patterns that are approximately omnidirectional, like a linear wire antenna. The polarization of the slot antenna is generally linear. The slot size, shape and what is behind it offer design variables that can be used to tune performance [14].

Consider an infinite conducting sheet, with a rectangular slot cut out of dimensions a and b, as shown in Figure 1.3. If some reasonable fields in the slot can be excited (often called the aperture), then a slot antenna is obtained.

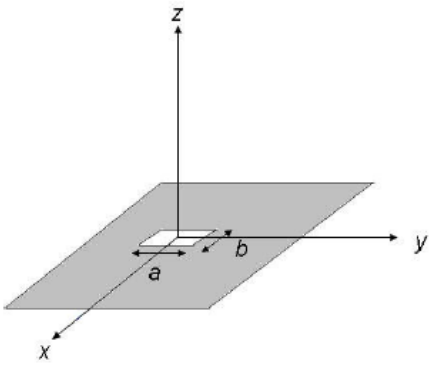

Figure 1.3 Rectangular Slot antenna with dimensions *a* and *b* [13].

Babinet's principle relates the radiated fields and impedance of an aperture or slot antenna to that of the field of its dual antenna. The dual of a slot antenna would be if the conductive material and air were interchanged that is, the slot antenna became a metal slab in space. An example of dual antennas is shown in Figure 1.4.

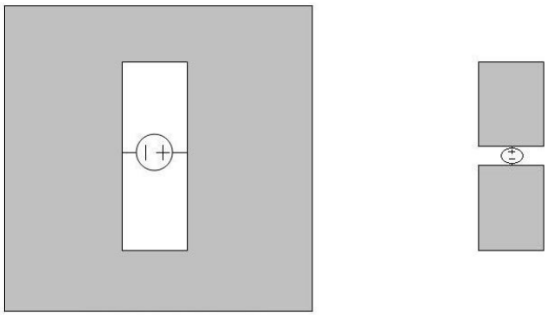

Figure 1.4 Dual antennas – Slot antenna (left), Dipole antenna (right) [13].

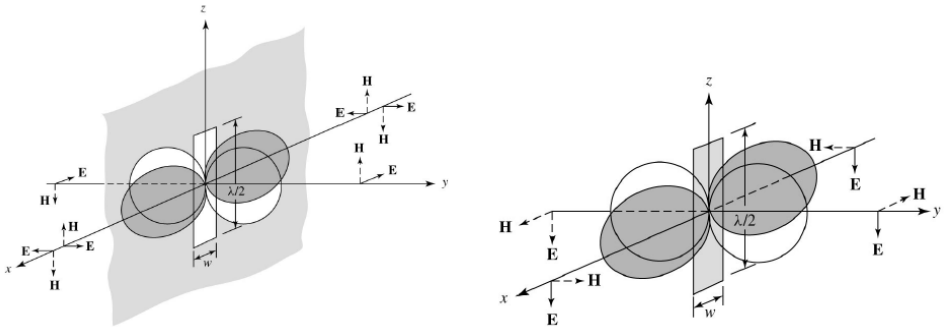

Figure 1.5 Comparison of slot antenna (left) and dipole antenna (right) [2].

It is important to note that the polarization of the two antennas are reversed. That is, since the dipole antenna on the right in Figure 1.4 is vertically polarized, the slot antenna on the left will be horizontally polarized.

1.2 Characteristics

Antennas are considered fundamental elements of radio communication and plays an important role in communication system. As well as other radio communication devices, the antenna has inherent properties and parameters which compromise its design and implementation. Some basic parameters of microstrip antennas will be described in the following sections.

1.2.1 Input impedance and Impedance bandwidth

Input impedance is the impedance which can be measured at the terminals of the antenna. It consists of the radiation resistance R_Σ (when multiplied by the squared input current I_{in}^2, real radiated power is obtained), of the loss-making resistance R_{loss} ($R_{loss} I_{in}^2$ equals to the power which is converted to heat in the antenna and around it). Radiation resistance and radiation reactance form the radiation impedance together [5].

The input impedance is measured with respect to some transmission line or source characteristic impedance. When both are not the same, a voltage wave is reflected, ρV, where ρ is the voltage reflection coefficient. Reflection coefficient at the input is also known as S_{11} or return loss and can be calculated by [6]

$$S_{11} = \frac{Z_A - Z_0}{Z_A + Z_0} \ [-], \tag{1.1}$$

where Z_A is the antenna impedance and Z_0 is the measurement characteristic impedance. It is typically expressed in logarithmic form as

$$S_{11dB} = 20 \cdot \log S_{11} \ [dB]. \tag{1.2}$$

Voltage standing wave ratio (VSWR) is another way to describe how well the antenna is impedance matched and is expressed as a function of the reflection coefficient by [2]

$$VSWR = \frac{1 + |S_{11}|}{1 - |S_{11}|} \ [-]. \tag{1.3}$$

Impedance bandwidth (IBW) is usually defined as a frequency range where 90% of supplied energy is absorbed by the antenna (10% of the energy is reflected back to the generator). The described situation corresponds approximately to VSWR equal to 2, from which it is possible to deduce the magnitude of reflection coefficient -10 dB [5]. Consequently, impedance bandwidth represents the frequency interval at which S_{11} magnitude is below -10 dB as shows Figure 1.6.

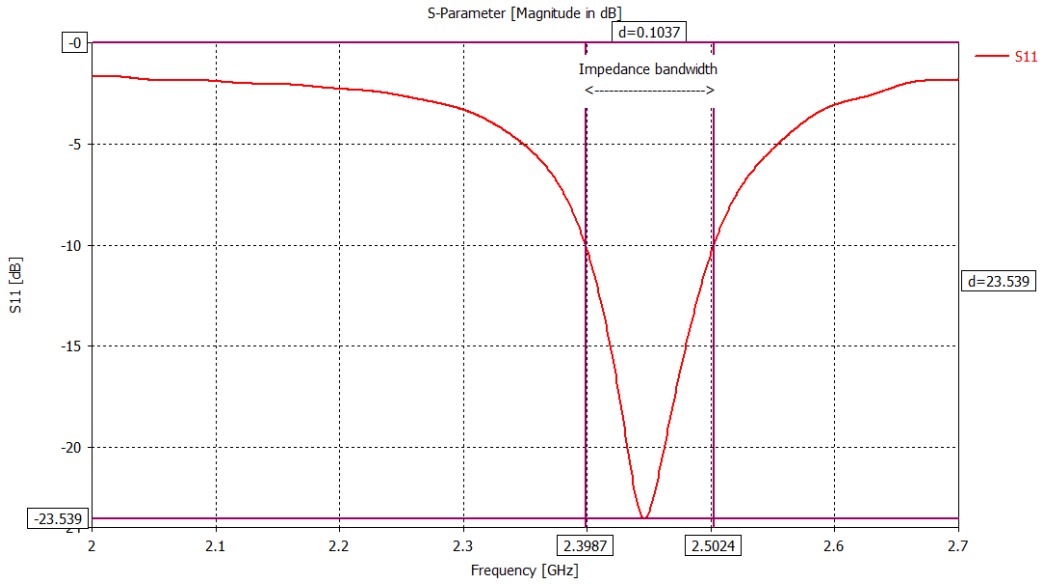

Figure 1.6 Impedance bandwidth of a square microstrip patch antenna with CP at 2.45 GHz frequency band.

An antenna can be looked from two points of view: circuit and spatial. From a circuit point of view the antenna behaves as a frequency filter because outside its operating frequency reflects back a lot of power, as shown in Figure 1.6.

1.2.2 Radiation pattern, Directivity factor and Directivity pattern

Now, let us take a look at the antenna from a spatial point of view – radiation pattern. The radiation pattern is a key characteristic that describes several quantities, such as directivity, gain, electric field or radiation vector of an antenna. It is a graphic representation of the properties of the energy radiated from the antenna into its surrounding [5]. The radiation pattern is determined in the far field region and is represented as a function of the directional coordinates, where radiation fields E and H are perpendicular to each other and transverse to the direction of propagation [2]. In order to describe it, the spherical coordinate system is used, where each direction is described by two angles: azimuth (φ) and elevation (ϑ), as shown in Figure 1.7.

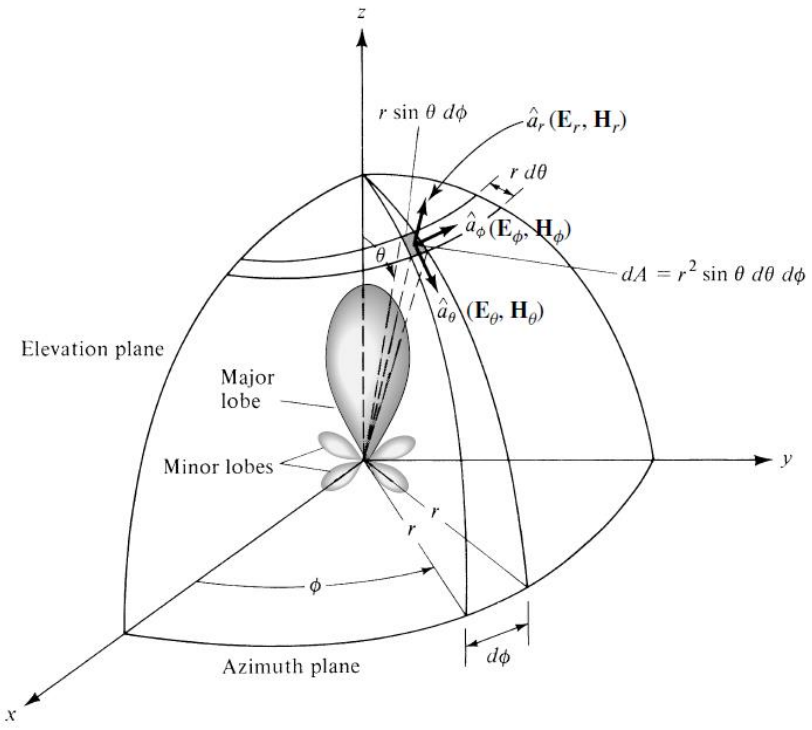

Figure 1.7 Antenna spherical coordinate system – azimuth φ (0° - 360°), elevation ϑ (-90° - 90°) [2].

Radial distance of the far field (Fraunhofer) region is defined by [2]

$$R_{ff} = \frac{2D^2}{\lambda}\ [m], \tag{1.4}$$

where D is the largest dimension of the antenna [m][1] and λ is the wavelength [m].

The Poynting vector S describes both the direction of energy propagation of a plane wave and the power density of an electromagnetic wave, defined as [6]

$$S = E \cdot H^*\ [W/m^2], \tag{1.5}$$

where E is the electrical field vector [V/m] and H^* is the complex conjugate vector of the magnetic field phasor [A/m].

The directivity factor D (φ, ϑ) describes and quantifies antenna radiation. The directivity factor is greater than 1 for those directions where radiation is concentrated by the antenna, and less than 1 for those directions where the radiation is suppressed. Moreover, the directivity factor of an isotropic radiator is equal to 1 for all its directions [5]. In mathematical form, D is written as [2]

$$D\ (\varphi, \vartheta) = \frac{U}{U_0} = \frac{4\pi U}{P_{rad}}\ [-]. \tag{1.6}$$

If the direction is not specified, it is understood that the direction of maximum radiation intensity D_{max} (maximum directivity), expressed as [2]

[1] Note: D must be large compared to λ ($D > \lambda$).

$$D\ (\varphi,\vartheta)_{max} = \frac{U_{max}}{U_0} = \frac{4\pi U_{max}}{P_{rad}}\ [-], \tag{1.7}$$

where U is the radiation intensity [W/unit solid angle], U_{max} is the maximum radiation intensity [W/unit solid angle], U_0 is the radiation intensity of the isotropic source [W/unit solid angle] and P_{rad} is the total radiated power [W].

The directivity pattern is a graphic representation of directional properties of the antenna. Directional properties are typically expressed in the form of the absolute value of the radio of electric intensity of the radiated wave in a given direction and its maximum value, which are computed for the far field of the antenna [5]. The directivity pattern is usually represented in 2D view (Polar and Cartesian system coordinates) for a specific plane. Figure 1.8 shows directivity pattern for the antenna in reference to Figure 1.6.

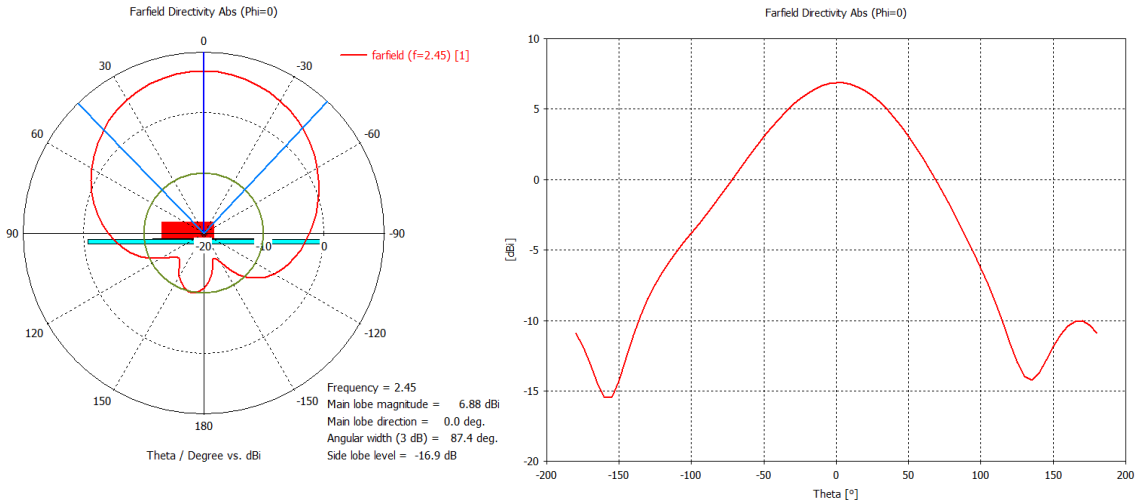

Figure 1.8 Polar and Cartesian representation of directivity pattern for a square microstrip patch antenna with CP for 2.45 GHz frequency band.

1.2.3 Gain and Efficiency

The antenna gain, also called the absolute gain G_{abs}, is the maximum value of the directivity factor expressed in decibels as [5]

$$G_{abs} = 10 \cdot \log D_{max}\ [dB]. \tag{1.8}$$

The antenna efficiency η is defined as the ratio between the radiated power and the input power. It can be simply deduced from the relation [5]

$$\eta = \frac{R_{\Sigma in}}{R_{\Sigma in} + R_{loss}}\ [-], \tag{1.9}$$

where $R_{\Sigma in}$ is the radiation resistance related to input current, and R_{loss} is the lossy resistance related to input current.

Good antenna efficiency is conditioned by a small lossy resistance and (or) by a high radiation resistance, whilst low efficiency is presented in antennas of small radiation resistance[2] [5].

[2] Note: These types of antennas are considerably shorter than the wavelength [5].

1.2.4 Bandwidth

The bandwidth (BW) of an antenna is defined as the range of frequencies, where the antenna characteristics (such as input impedance, radiation pattern, beamwidth, polarization, gain, directivity, efficiency) are within an acceptable value of those at center frequency. Bandwidth can be expressed in percentage terms as [2]

$$\mathrm{BW} = \frac{f_{max} - f_{min}}{f_0} \cdot 100\ [\%], \tag{1.10}$$

where f_{max} is the higher frequency (maximum), f_{min} is the lower frequency (minimum) and f_0 is the center frequency – all frequencies expressed in [Hz].

The most common bandwidths are: Impedance bandwidth (IBW) measured below -10 dB reference, axial ratio bandwidth (AR BW) measured below 3 dB reference and gain bandwidth (GBW) measured by -3 dB cutoff frequency.

1.2.4.1 Effect of dielectric substrate on bandwidth

The dielectric substrate creates a supporting pad, on which are different shapes of patch elements are applied, and consequently, it is a basic construction element with both physical and mechanical inherent properties, which affect the overall realization of a microstrip antenna. Important parameters of a dielectric substrate are: the dielectric constant ($2.2 \leq \varepsilon_r \leq 16$), and the dielectric loss tangent ($0.0001 \leq \tan\delta \leq 0.06$) or imaginary part of the dielectric constant [7].

Figure 1.9 and Figure 1.10 show the bandwidth and surface wave loss dependence, respectively, on dielectric substrate thickness for different common relative permittivity values. From both graphs it can be observed that the bandwidth increases with increasing dielectric substrate thickness, on the contrary, antenna efficiency decreases with increasing dielectric substrate thickness. This dependence is described by the antenna quality factor *Q*.

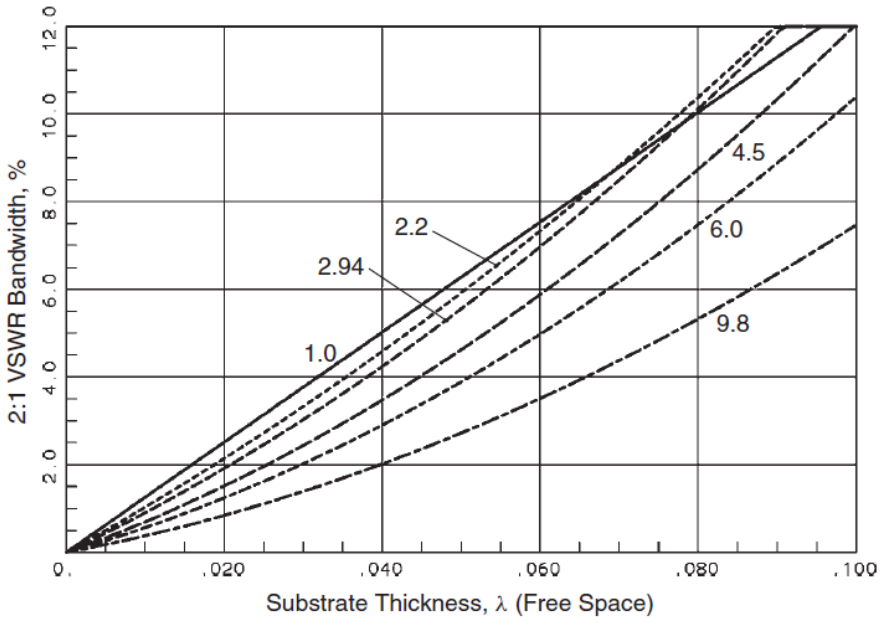

Figure 1.9 Effect of the dielectric substrate thickness on the bandwidth for different dielectric substrate constants [6].

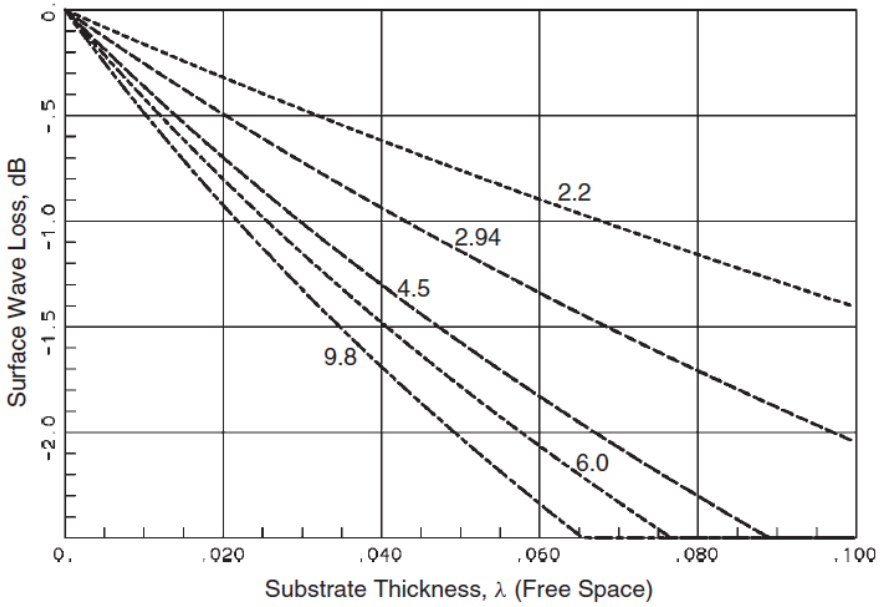

Figure 1.10 Effect of the dielectric substrate thickness on the surface wave loss for different dielectric substrate constants [6].

1.2.4.2 Wideband microstrip planar antennas

In Section 1.1, several useful features and advantages of microstrip planar antennas were detailed. Nevertheless, a considerable disadvantage was as well stated – a narrow bandwidth (typically of around 1-5%). The narrow impedance and radiation bandwidth are the primary disadvantages which are caused mainly by frequency-dependent efficiency, radiation direction or polarization [7].

If we compare this bandwidth with typical wire antennas and waveguides, which commonly reach bandwidth in a range of 15-50%, reached bandwidth with microstrip planar antennas is in fact considerably narrow. For this reason, much effort has been dedicated to the research and development of broadband techniques, as is presented in subsequent section.

Table 1.2 shows the required bandwidths of today's wireless communication systems.

Table 1.2 Summary of wireless communication systems and bandwidths [4].

	Frequency [MHz]	Bandwidth [%]
GSM	890 - 960	7.6
DCS	1710 - 1880	9.5
PCS	1850 - 1990	7.5
UMTS	1920 - 2170	12.2

1.2.4.3 Bandwidth enhancement techniques

Following are some techniques for increasing bandwidth on a microstrip antenna:

Table 1.3 Broadband techniques for microstrip planar antennas [7].

Approach	Techniques
Lower the *Q*	Select the radiator shape
	Thicken the substrate
	Lower the dielectric constant
	Increase the losses
Use impedance matching	Insert a matching network
	Add tuning elements
	Use slotting and notching patches
Introduce multiple resonances	Use parasitic (stacked or co-planar) elements
	Use slotting patches, insert impedance networks
	Use an aperture, proximity coupling

1.2.5 Polarization

Polarization describes the orientation of the electric field intensity vector of an electromagnetic wave[3] [5]. Depending on how the electric field is oriented, 3 types of polarization are met: linear, circular and elliptical.

1.2.5.1 Linear polarization

If the electric field vector at a given point in space is always oriented along the same line at each instant of time, we can say that the electromagnetic wave is linearly polarized at that point. Some of its features are [2]:

- Only one component in one direction.
- Two linear orthogonal components are in time phase or 180° (or multiples of 180°) out of phase.

1.2.5.2 Circular polarization

The electric field vector at a given point in space traces a circle as a function of time. The necessary and sufficient conditions to achieve this are [2]:

- The field vector must have two linear and orthogonal components.
- The two components must have the same magnitude.
- The two components must have both time and phase difference of odd multiples of 90°.

Depending on the direction of the phase shift, circular polarization can be classified into two types: Right hand circular polarization (RHCP) and left hand circular polarization (LHCP).

1.2.5.3 Elliptical polarization

An electromagnetic wave is elliptically polarized if the electric field vector traces an

[3] Note: If the direction is not stated, it is taken the polarization in the direction of the maximum gain.

ellipse. The necessary and sufficient conditions to achieve this are [2]:

- The field vector must have two linear orthogonal components.
- The two components can have the same or different magnitude.
- If the two components are not of the same magnitude, the time-phase difference between the two components should not be 0° or multiples of 180° (then we would have linear polarization).
- If the two components are of the same magnitude, the time-phase difference between the two components should not be multiple of 90° (then we would have circular polarization).

1.2.5.4 Generation of circular polarization in microstrip antennas

The principle of obtaining a circular polarization, as stated in Section 1.2.5.2, is by exciting two orthogonal modes with a 90° time-phase between them. This step can be achieved by slightly modifying the physical dimensions of the patch and using either single, or two, or more feeds arrangements [6].

A square patch element can be easily excited to obtain an ideal circular polarization by feeding the element at two adjacent edges as shows Figure 1.11. It consists of exciting the two orthogonal modes in the following way: the TM_{010} with the feed at one edge and TM_{001} with the feed at the other edge. The quadrature phase difference is obtained by feeding the element with a 90° power divider or 90° hybrid [2].

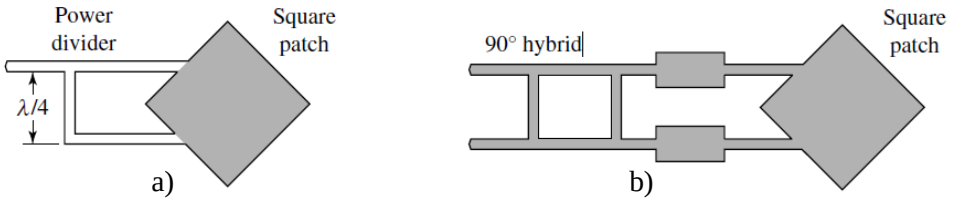

Figure 1.11 Rectangular patch feed arrangements for circular polarization – a) At adjacent sides through a power divider, b) At adjacent sides through a 90° hybrid [2].

On the other hand, circular polarization for the TM_{110} can be obtained in a circular patch element by using two feeds with an appropriate angular separation. An example is shown in Figure 1.12, where it can be observed that two coax feeds separated by 90° generate fields that are orthogonal to each other under the patch likewise outside the patch [2].

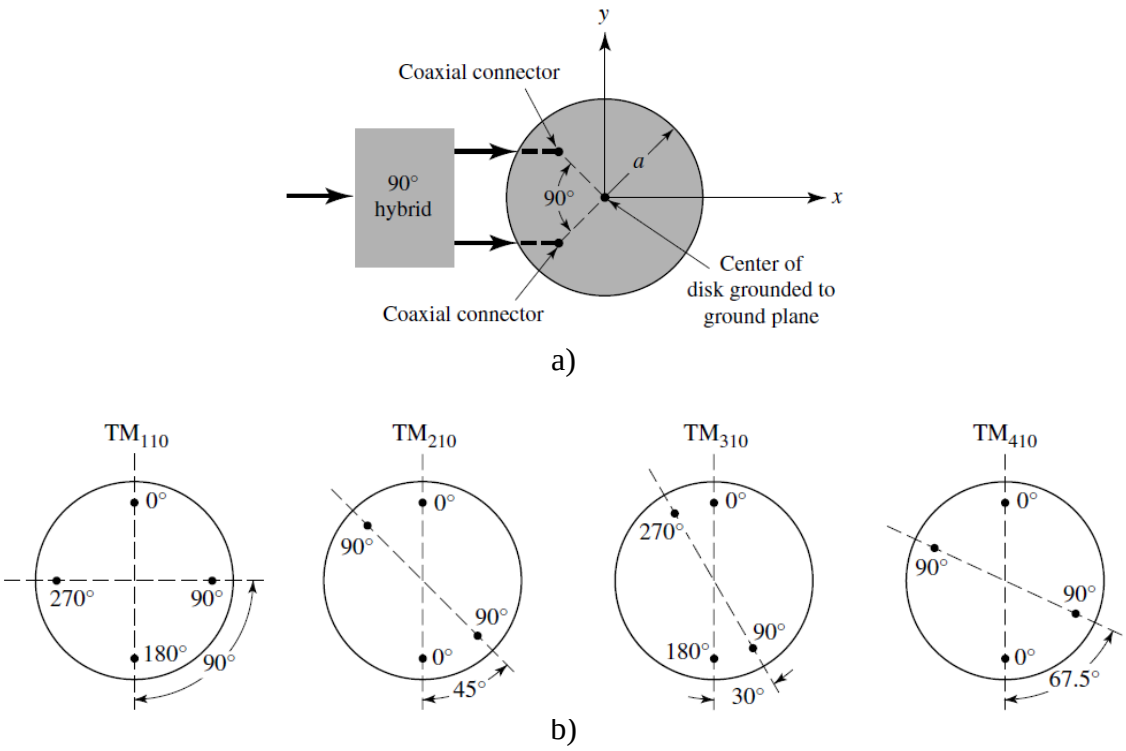

Figure 1.12 Circular patch feed arrangements for circular polarization – a) Feed with coaxial connector, b) Arrangement for TM_{110} and higher modes [2].

1.2.6 Axial ratio

The axial ratio (AR) is the relationship between the orthogonal components of an electric field – the maximum and minimum electric field intensity vector E in one period, used to describe how close the polarization is circular and defined by [2]

$$AR = \frac{E_{max}}{E_{min}} \ [-], \tag{1.11}$$

which is usually expressed in decibel units as

$$AR_{dB} = 20 \cdot \log\left(\frac{E_{max}}{E_{min}}\right) \ [dB]. \tag{1.12}$$

Due to polarization types, the axial ratio can take values from 1 to infinity. Values in the different polarizations are[4] [2]:

- Circular polarization: 1 (0 dB).
- Elliptical polarization: greater than 1 (> 0 dB).
- Linear polarization: infinite, because the orthogonal components of the electric field are zero.

[4] Note: These values are theoretical, AR in an antenna tends to degrade away from the main beam.

1.3 Feeding

Feeding is a key component when performing the design of an antenna. There are several configurations to feed microstrip antennas. However, the most popular feeds are: microstrip line, coaxial probe, aperture coupling and proximity coupling [2].

1.3.1 Microstrip line feed

This consists of a microstrip line connected directly to the radiation patch. Both of them are printed on the same substrate [2]. This feed has the following qualities:

- Easy to fabricate and match – the simplest type of feed.
- Control of input impedance.
- Generates higher order modes which produce cross-polarized radiation.
- Thick substrates produce surface waves and spurious feed radiation.
- Same substrate is used for patch and feeding line.
- Easy to model.
- Narrow bandwidth – typically 2-5%.

1.3.2 Coaxial probe feed

This consists of an inner conductor attached to the radiation patch and an outer conductor connected to the ground plane [2]. This feed has the following qualities:

- Easy to fabricate and match.
- Control of input impedance – through inductive impedance with thick dielectric.
- Generates higher order modes which produce cross-polarized radiation.
- Low spurious radiation.
- Difficult to model – specially for thick substrates ($h > 0.02\lambda_0$)
- Narrow bandwidth.
- Its placement requires to hole the substrate and soldering.

1.3.3 Aperture coupling feed

This consists of two substrates separated by a ground plane. There is a microstrip feed line placed on the bottom of the lower substrate whose energy is coupled to the patch through a slot on the ground plane, which separates both substrates [2]. This feed has the following qualities:

- Most difficult fabrication.
- Control of input impedance – through width of the feeding line and the length of the slot.
- Good polarization purity and no cross-polarized radiation in the principal planes.

- Moderate spurious radiation.
- Different substrate is used for patch and line.
- Easy to model.
- Narrow bandwidth.

1.3.4 Proximity coupling feed

As aperture coupling feed, proximity coupling feed also does not use direct contact of the feeding line with the patch. Instead, it utilizes an electromagnetic coupling between the feeding line and the patch, both printed on separated substrates [2]. This feed has the following qualities:

- Difficult fabrication.
- Control of input impedance – through length of the feeding stub and the width-to-line ratio of the patch.
- Low spurious radiation.
- Different substrate is used for patch and line.
- Easy to model.
- Widest bandwidth (nearly 13%).

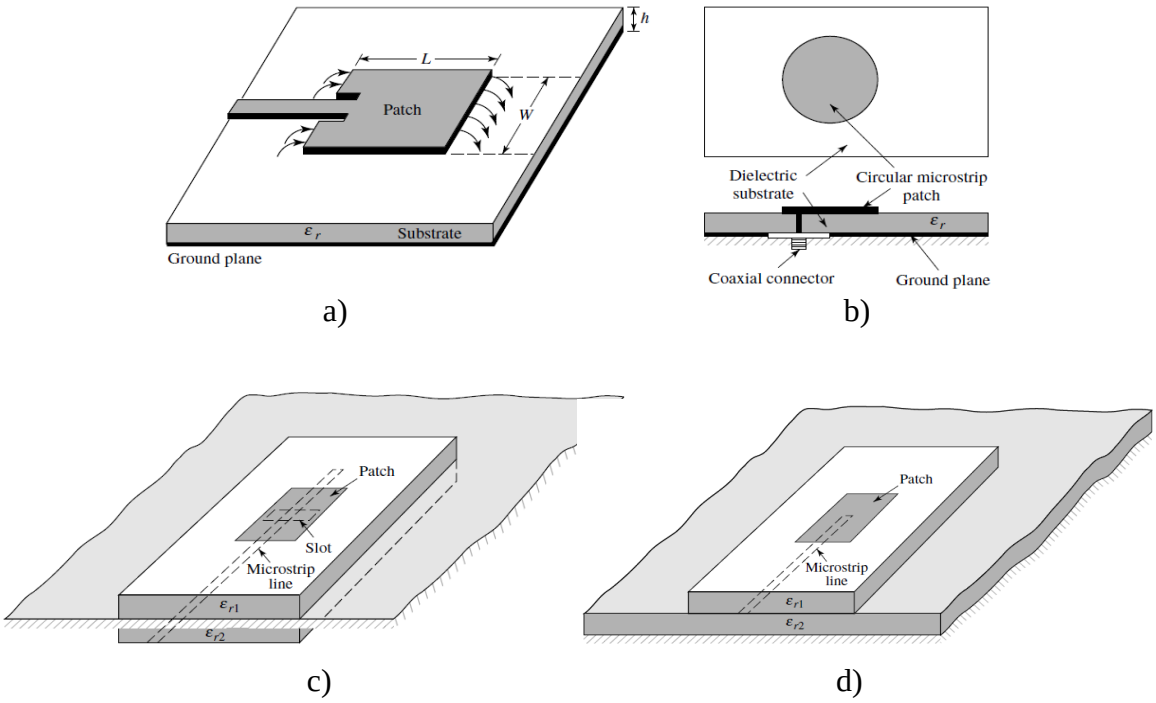

Figure 1.13 Typical feeds for microstrip antennas – a) Microstrip line feed, b) Coaxial probe feed, c) Aperture-coupled feed, d) Proximity-coupled feed [2].

1.4 Microstrip planar antennas with SIW cavity resonator

As highlighted in Section 1.1.1, microstrip planar antennas are characterized by a narrow impedance bandwidth. Despite many several advantages, such as small size, low weight and low cost, this is the major obstacle to their utilization in broadband applications.

On the other hand, the literature [8] refers to one method of increasing the bandwidth of a microstrip planar antenna by placing a patch in a substrate integrated waveguide (SIW) cavity resonator. In the same literature, it is revealed that this type of resonator has a positive effect on reducing losses, suppressing parasitic surface waves and reducing bonding between patches in a row or field.

The SIW cavity resonator is based on a substrate integrated waveguide, which is a technology developed in the late 1990s and very much used and studied in recent years because of its similar advantages to conventional metallic rectangular waveguides – high quality factor, high power capacity, and self-consistent electric shielding [9]. For this reason, the SIW has high level integration to millimeter and centimeter wave technologies for components such as filters, oscillators, antennas, directional couplers, etc. It consists of the formation by two rows of periodically distributed vias with center-to-center distance embedded into the dielectric substrate and by a metalized cladding at the top and bottom of the dielectric substrate [9]. This mechanical construction is illustrated in Figure 1.14.

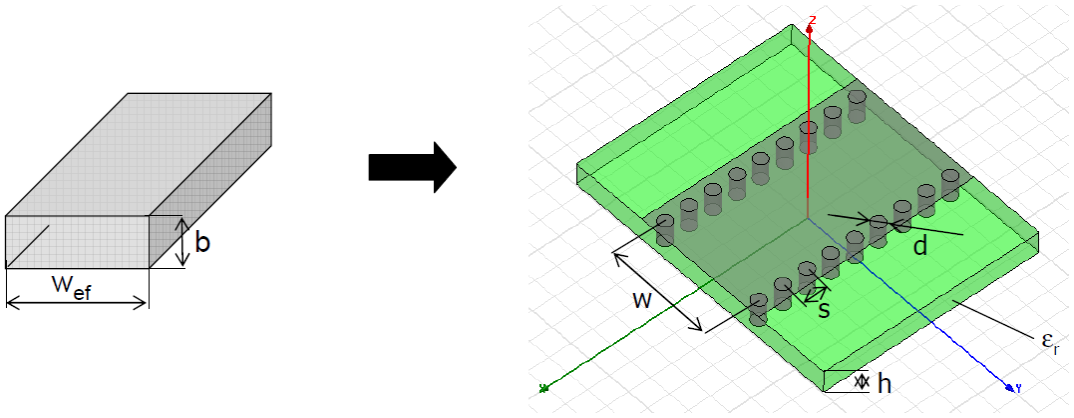

Figure 1.14 Transition from a rectangular waveguide to a substrate integrated waveguide [10].

As was stated, SIW properties are very similar to a rectangular waveguide[5], however, in the SIW only TE_{m0} modes exist (TM modes does not exist). The width of the equivalent rectangular waveguide can be approximately calculated by [10]

$$w_{ef} = w - 1.08\frac{d^2}{s} + 0.1\frac{d^2}{w}\ [m]. \tag{1.13}$$

The cutoff frequency of SIW dominant mode TE_{10} can be approximately calculated (with high precision) by [10]

$$f_{cutoff}^{TE_{10}} = \frac{c}{2\sqrt{\varepsilon_r} w_{ef}}\ [Hz]. \tag{1.14}$$

[5] Note: A disadvantage is the possible attenuation and leakage of the signal caused by the hole vias.

For a proper design, the following ratios are recommended [10]

- $s/d < 2$.
- $d/w < 1/8$.

1.5 Planar circular array

Planar antenna arrays are mainly used to improve directivity pattern (high gain), which is often demanded for applications within long distance communication, as well as to cancel co-channel interferences. This aim cannot be accomplished only by a single element, but requires an assembly of radiating elements in an electrical and geometrical configuration for such a purpose. Based on topology they can be linear, circular, planar or conformal, and based on energy they can be broadside, end-fire, phased and parasitic.

A circular array, in which the elements are placed in a circular ring commonly phased between them, is a type of array with several important applications such as span radio direction finding, air and space navigation, underground propagation, radar, sonar, and other many other systems [2].

Furthermore, another key point to comprehend the concept of the investigated antenna of the present work, and explained in Section 1.6, is that a parasitic array consists of an arrangement of elements which resonates with no connection to source (no current excitation by their own), and radiates power from other resonating elements. Such elements are known as parasitic elements and play an important role in the overall performance of the entire antenna system [2].

1.5.1 Array factor

A general diagram of circular array is shown in Figure 1.15 for a *N*-element array. The radius of the array is *a*. The angle between elements is assumed to be uniform, such that

$$\Delta\phi = \phi_{n+1} - \phi_n = \frac{2\pi}{N}. \tag{1.15}$$

In this case, the position vector of the *n*th element can be written as

$$r'_n = a\cos\phi_n\hat{x} + a\sin\phi_n\hat{y}, \tag{1.16}$$

where

$$\phi_n = n\Delta\phi\,\frac{2\pi}{N}n. \tag{1.17}$$

Thus, the array factor (AF) can be written as [2]

$$AF = \sum_{n=0}^{N-1} I_n e^{jka[\cos(2\pi n/N)\sin\theta\cos\phi + a\sin(2\pi n/N)\sin\theta\cos\phi]}\ [-], \tag{1.18}$$

where ϕ_n is the angular position of the nth element on *x*-*y* plane and I_n is the amplitude excitation of the *n*th element.

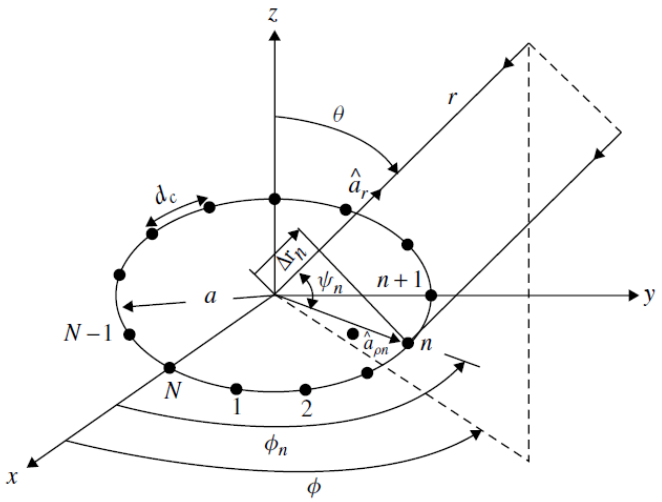

Figure 1.15 Geometry of uniform circular array of *N* elements [2].

2 PRACTICAL PART

2.1 Antenna design and optimization

This section is focused on the antenna design concept and its operating mechanism proposed in the primary literature of this work [1]. Critical aspects, such as the antenna configuration, the customized parasitic element and its array, and the SIW cavity resonator embedded in the antenna are examined. Furthermore, this section explores the respective stages performed in the full-wave program CST Microwave Studio (CST MWS) version 2018 for design and optimization. The simulations for verifying the antenna properties were performed for 3 different dielectric substrates: Taconic TLX – for verification of published results in the literature as initial model design, Arlon CuClad 217 – which was initially assigned for the redesign in the first stage of this work, and Rogers 5870 – which was later chosen for fabrication in the second stage due to better technology conditions for its implementation than Arlon CuClad 217. Moreover, techniques used for optimization procedure for both substrates are mentioned.

2.1.1 CST Microwave Studio

CST MWS is a powerful simulation platform dedicated to fast and accurate 3D electromagnetic simulation of high frequency components in Time Domain (Transient) Solver, as well as Frequency Domain Solver. For reaching a high accuracy it uses Finite Integrate Technique (FIT) with features such as Perfect Boundary Approximation (PBA), Thin Sheet Technique (TST) and Multilevel Subgridding Scheme (MSS) [11].

2.1.2 Design

The investigated antenna consists fundamentally of a shortened monopole patch, an annular ring slot array, and a SIW cavity resonator. Figure 2.1 exhibits the customized parasitic patch element and the total geometry of the antenna. Moreover, antenna parameters and their values are presented in Table 2.1.

As observed in Figure 2.1, the customized parasitic patch element of the antenna is comprised of a set of sub-elements such as a phase compensatory line (2.), a shorted annular ring slot (3.), and a shorting via (4.), which is in the sectorial patch arrangement. The phase compensatory line and the parasitic patch in the antenna meet with a cross formation where the parasitic patch is set.

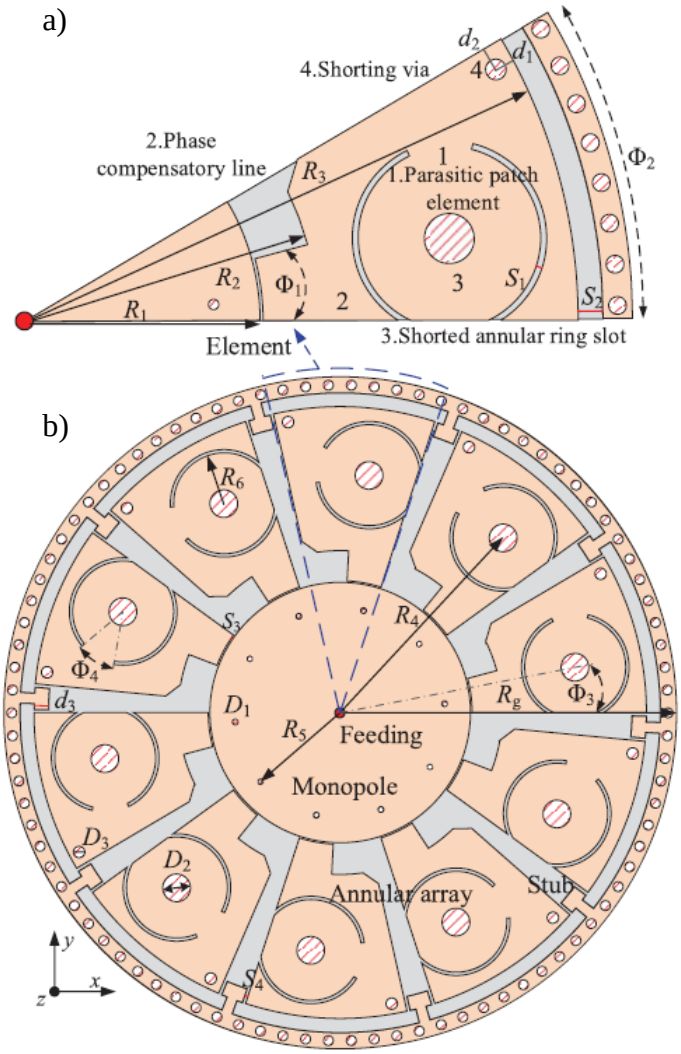

Figure 2.1 Antenna prototype – a) Customized parasitic patch element, b) Total antenna structure with annular array [1].

Table 2.1 Parameters of the antenna – Length [mm] and angle [°] [1].

Parameter	Value	Parameter	Value
R_1	16	D_1	0.7
R_2	19.9	D_2	3.4
R_3	37.6	D_3	1.4
R_4	29.4	S_1	0.4
R_5	12.9	S_2	1.7
R_6	6.2	S_3	0.2
R_g	41.3	S_4	0.35
Φ_1	15	d_1	1.3
Φ_2	30.6	d_2	1.6
Φ_3	11	d_3	1.8
Φ_4	40	-	-

The purpose of the conductive vias on the central monopole is to generate a fundamental TM_{01} mode at the operating frequency, where a resonant TM_{02} mode has previously occurred, and both modes together excite a wideband vertically polarized electric field E_θ. The current produced by these modes can be observed in Figure 2.2, where J_m is the radial directional current source.

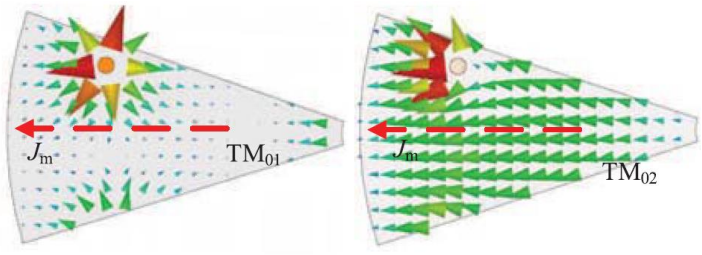

Figure 2.2 Current distribution on the central monopole patch at the TM_{01} and TM_{02} resonant modes [1].

The symmetric arrangement of the central monopole structure causes the currents from the shorting vias to be canceled in the φ-direction, and consequently the radial directional component will be the only current source to work as an effective radiator. At the same time, energy from the monopole will flow through customized parasitic patch element through the phase compensatory line. Because a shorted annular ring slot is not etched on the element, the current on the line will flow far away from the radial direction once the element and the annular ring couple together. This will originate a wideband horizontal polarization E_φ at the same frequency, and as result of the orthogonal joint between E_θ and E_φ, a circular polarization wave will be obtained (See Section 1.2.5.4). Thus, multiple identical customized parasitic elements are introduced as an array radiator to produce a wideband E_φ field. In view of this, both orthogonal linear components excited from the monopole patch and the customized parasitic array, respectively, produce in the vertical plane a circularly polarized conical-beam radiation pattern with high gain.

As explained in the previous paragraph, a CP radiation pattern is achieved in the antenna. In addition to this, an in-phase loop current (referred to as slot sloop current J_p) will appear on the annular array under control of each annular ring slot. Nevertheless, the frequency shift will be far away from the slot loop current, and as a result the annular ring slot will not behave as a resonator. Hence, in order to generate another φ-directional linear polarized component for a wideband CP antenna a shorting via at the end of the parasitic patch and a small stub, which connects to SIW cavity resonator edge, are introduced.

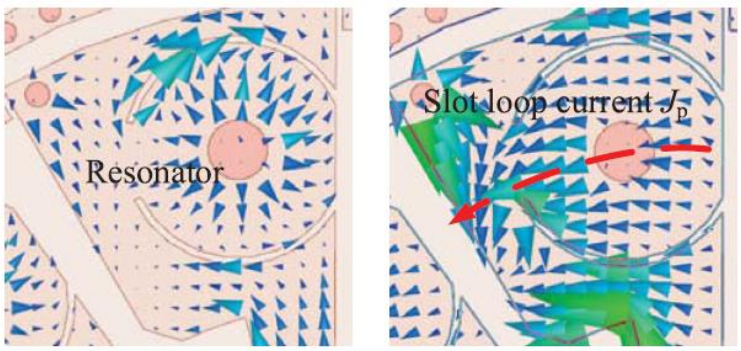

a) b)

Figure 2.3 Surface current distribution on the customized parasitic patch element at different times – a) $t = 0$, b) $t = T/4$. T is the period of oscillation at 5.9 GHz.

The antenna is fed by a coaxial probe in the center of the antenna within a SIW cavity resonator. The used SIW cavity resonator consists of shorting vias and multiple small stubs (each shorting vias is arrayed next to a small stub). This type of SIW cavity resonator is applied as a compensatory capacitor at high frequency and as a signal filter to work in the cavity. Presented results in the literature [1] revealed that the reflection coefficient curve shifts to the low frequency without SIW cavity. In addition to this characteristic, it is also demonstrated that gain in the φ-direction almost linearly decreases as the frequency increases without SIW cavity, meanwhile when the SIW cavity is applied the curve becomes smoother.

Furthermore, the SIW cavity is not only convenient in the antenna structure for tuning the amplitude and phase of the slot loop current, but it also brings several resonant modes in a relatively narrow band. It plays a crucial role, together with the size parameters of the stubs, for axial ratio and high gain performance. Thus, by using ten element radiators, a smooth high gain performance can be obtained in terms of gain-φ and gain-θ

According to the analysis in the literature [1], the presented SIW cavity-backed patch antenna should be analyzed in a "view of mutual coupling resonant patch mode" rather than the cavity mode, because of the surface current of the cavity, which does not flow on the surface created by the parasitic array. Moreover, it is stated an important advantage – a large ground compatibility, because of the less sensitivity of the monopole patch and the customized parasitic array to the size of the ground plane. This implies that a possible change of ground plane size in the antenna design will not affect the two resonant modes except for the AR elevation angle and the radiation patterns.

This type of circularly polarized conical beam spherical slot array antenna is studied in [14]. The integral equations of the unknown magnetic currents over the slots and electric current at the feed probe must be established. These equations are formulated base on the Field Equivalent Principle and enforcing the boundary condition as follows:

$$jW\varepsilon_0 \sum_{k=1}^{N_s} a_{sk} \left\{ \iint_{sl} \iint_{sk} \hat{m}_{sl} \cdot \left(\bar{\bar{G}}_{HM}^{in} + \bar{\bar{G}}_{HM}^{out} \right) \cdot \hat{m}_{sk} dS_{sk} dS_{sl} \right\} + b_f \iint_{sl} \int_{f} \hat{m}_{sl} \cdot \bar{\bar{G}}_{HJ}^{in} \cdot \hat{j}_f dl_f dS_{sl} = 0 \tag{2.1}$$

$$\sum_{k=1}^{N_s} a_{sk} \int_{f} \iint_{sk} \hat{j}_f \cdot \bar{\bar{G}}_{EM}^{in} \cdot \hat{m}_{sk} dS_{sk} dl_f + jW\mu_0 b_f \int_{f} \int_{f} \hat{j}_f \cdot \bar{\bar{G}}_{EJ}^{in} \cdot \hat{j}_f dl_f dl_f = 1 \tag{2.2}$$

where l=1,2,…,N_s. The dyadic Green's functions inside and outside the concentric conducting spherical cavity enclosed by the conducting conical surface for electric and magnetic fields due to the magnetic and electric current sources are derived to fulfill the requirement of the integral equations.

In addition to this, [15] mentions that the distance d from the monopole to the center of the shorted annular ring slot can be calculated by

$$d = \frac{\lambda_0}{4 \cdot \sqrt{\varepsilon_e}}. \tag{2.3}$$

$$d = R_4 - R_1. \tag{2.4}$$

In addition to this, the circumference of the shorted annular ring slot can be calculated as

$$c = \frac{c_0}{f_0 \cdot \sqrt{\varepsilon_e}}. \tag{2.5}$$

$$c = 2\pi \cdot R_6 \cdot \frac{360 - \phi_4}{360}. \tag{2.6}$$

where λ_0 is the wavelength in free space and ε_0 is the effective permittivity, f_0 is the centre resonant frequency and c_0 is the speed of light in vacuum. R_1, R_4, R_6 and ϕ_4 are parameters of the presented antenna, which can be appreciated in Figure 2.1.

In CST MWS, the most important consideration in the design of such a complex type of the antenna presented in this work was to parameterize all dimensions in the parameter list of the program. This allows creation of dependencies between parameters in the antenna structure during its design which are then used to modify both specific antenna components and (or) the entire layout. Parameter names and referral values from the literature were employed for the first design, as shown in Figure 2.4.

Parameter List

Name	Expression	Value	Description
Rg	= 41.3	41.3	Radius of entire antenna
ts	= 3	3	Substrate thickness
t	= 0.036	0.036	Cladding thickness
R1	= 16	16	Radius of monopole patch
R2	= 19.9	19.9	Radius up to phase compensatory line
R3	= 37.6	37.6	Radius up to shorting via
R4	= 29.4	29.4	Radius up to annular array
R5	= 12.9	12.9	Radius up to internal via of the monopole
R6	= 6.2	6.2	Radius of shorted annular ring slot
phi1	= 15	15	Angle in phase compensatory line
phi2	= 30.6	30.6	Angle of entire parasitic element
phi3	= 11	11	Angle in shorted annular ring slot
phi4	= 40	40	Angle of parasitic patch element
D1	= 0.7	0.7	Diameter of internal via of the monopole
D2	= 3.4	3.4	Diameter of internal via of the shorted annular ring slot
D3	= 1.4	1.4	Diameter of shorting via
S1	= 0.4	0.4	Width of annular ring element
S2	= 1.7	1.7	Width of outer circular sector on the annular array
S3	= 0.2	0.2	Width of outer circular sector on the monopole
S4	= 0.35	0.35	Width of rectangular element next to the stub
d_1	= 1.3	1.3	Radial position of the shorting via
d_2	= 1.6	1.6	Tangential position of the shorting via
d_3	= 1.8	1.8	Upper height of the stub

Figure 2.4 Parameter list of the antenna in CST MWS for initial design with Taconic TLX.

Secondly, it was essential in the creation of this symmetrical array to determine the part of the antenna which is repeated. For this reason, the approach was primarily to create a circular sector[6] of 36° with radius R_g = 41.3 mm, which will be duplicated nine times by the *Transform – Rotate* function, creating a total of 10 circular sectors coupled together around a common point (center point). As a result of this operation, the complete circular antenna shape was obtained. Figure 2.5 (a, b) shows the final design of the customized

[6] Note: In the literature this angle is 30.6° and not 36° because the sector of the stub is not considered.

parasitic patch element and the complete antenna, respectively.

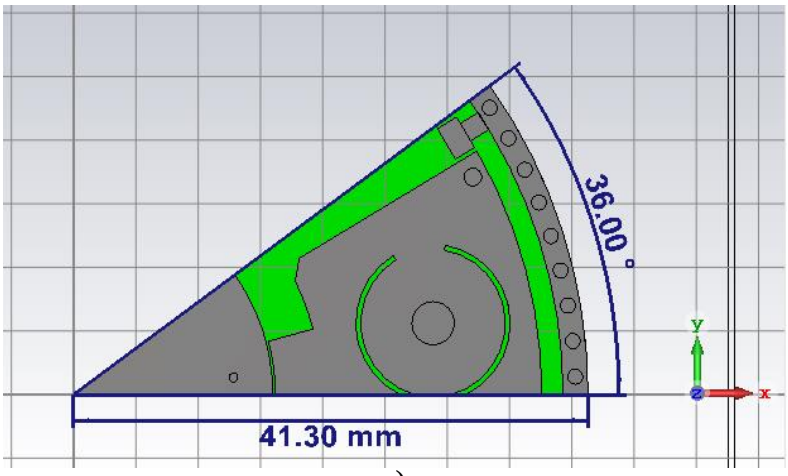

a)

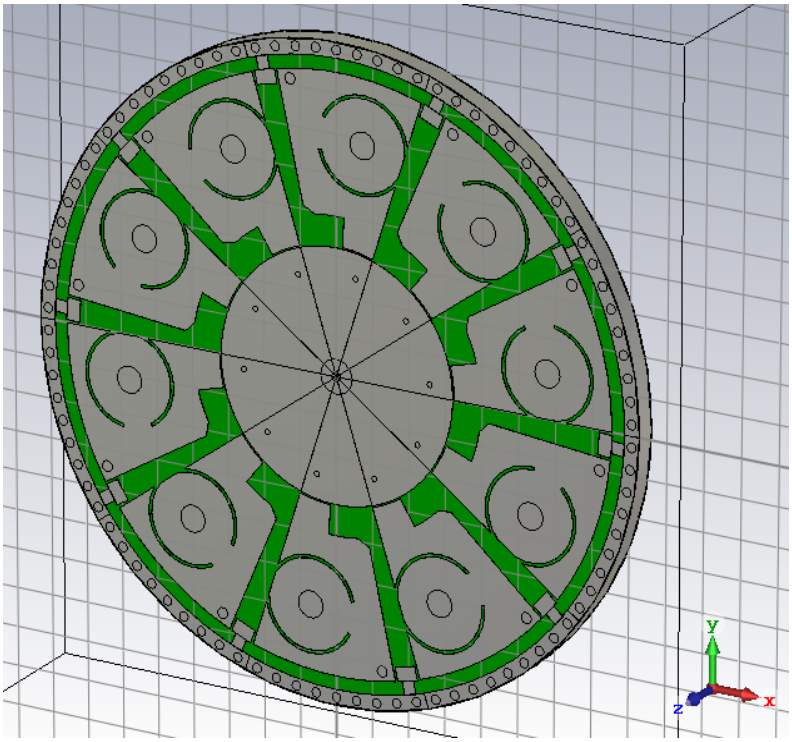

b)

Figure 2.5 Design of the antenna in CST MWS – a) Customized parasitic patch element, b) Complete antenna design with Taconic TLX substrate.

Thirdly, for designing the circular sector, it was necessary to previously define components such as the substrate for slot radiators (Taconic TLX) and the metallized cladding for the antenna (PEC). After that, the construction of components was accomplished by the *Modelling – Cylinder* function. The *Brick* function was used to create an object, which will be copied five times by the *Transform – Rotate* function, and after subtracted for each component by the *Boolean operation – Subtract* function. A half-circle shape was created after these operations, as shown in Figure 2.6. Finally, the brick was rotated 36° and the last step repeated for each component using the *Boolean operation – Intersect* function. Thus, a circular sector applied for the array design was obtained.

The overall design of the geometry and elements of the antenna are practically a subsequent creation of objects with help of Boolean operations such as addition, subtraction, multiplication, intersection and insertion. Figure 2.7 shows the SIW cavity resonator for feeding the slots in the antenna designed with some of these operations.

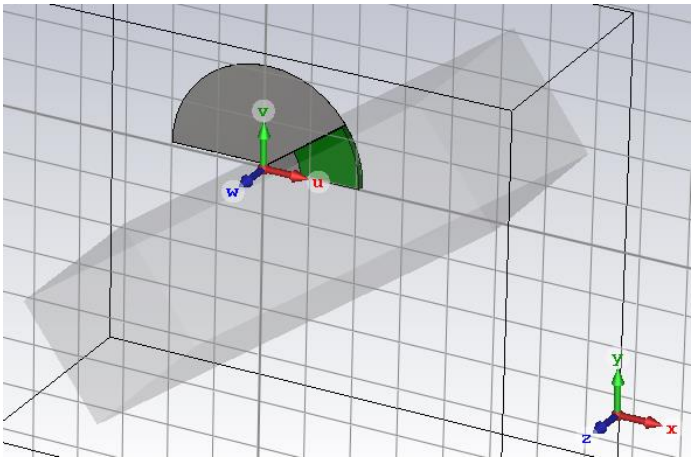

Figure 2.6 Brick creation method for customized parasitic element design.

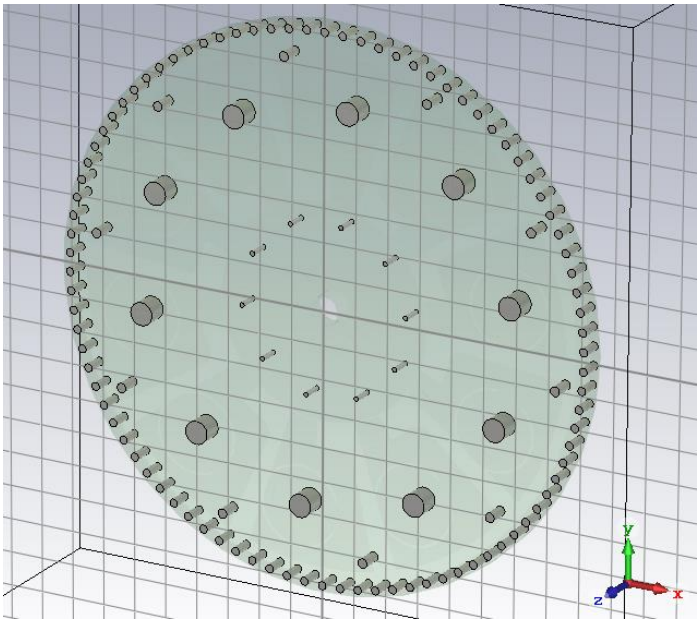

Figure 2.7 Design of the SIW cavity resonator embedded in the antenna.

For feeding the SIW cavity resonator, a coaxial probe was designed. The approach was to use the most realistic parameters for its construction. For this reason, typical dimensions for the coaxial connector associated with the antenna were considered (SMA-F-PP). A compromise between standard values for fabrication of this type of connector and a 50 Ω characteristic impedance was made for the calculation of dimensions. Equation 2.1 expresses the relation for calculating the coaxial cable impedance [12]

$$Z_0 = \frac{138}{\sqrt{\varepsilon_r}} \log\left(\frac{D}{d}\right) \ [\Omega]. \tag{2.7}$$

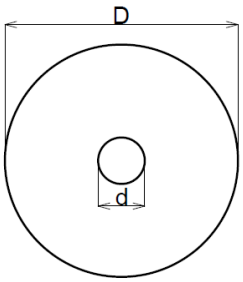

Figure 2.8 Cross-section of a coaxial connector.

Here, Z_0 is the characteristic impedance, D is the diameter of the outer conductor, d is diameter of the inner conductor and ε_r is the relative permittivity of dielectric between the conductors. Considering Teflon (ε_r = 2.1) as the dielectric material in the SMA connector and a standard inner pin diameter of d = 1.2 mm, D = 4.02 mm was obtained from Equation 2.1. Figure 2.9 shows the design of the coaxial feed and the dimensions of a typical SMA connector.

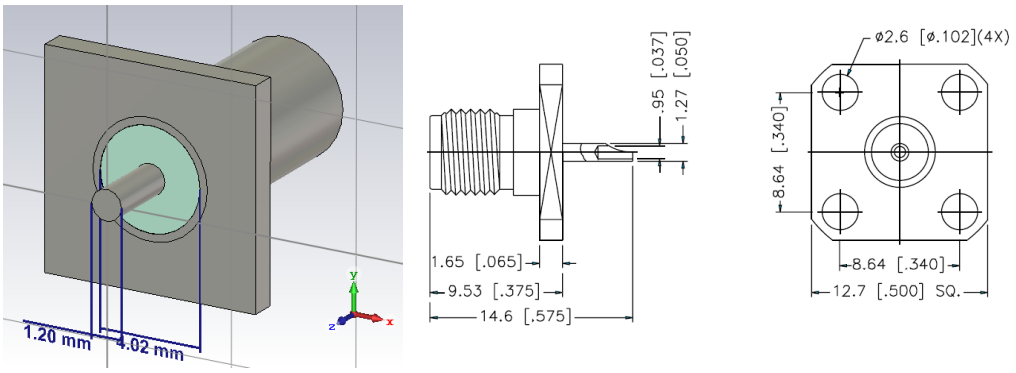

a) b)

Figure 2.9 a) Design of the coaxial feed, b) Real dimensions of a SMA connector.

2.1.3 Optimization

The antenna optimization was performed for dielectric substrates Arlon CuClad 217 and Rogers 5870 in terms of their following characteristics: impedance bandwidth, directivity patterns (gain) and axial ratio (below 3 dB for CP) for a 5.5 - 7 GHz frequency band. Optimization simulations were calculated on SIX server supported by FEEC BUT.

The approach to attain a high optimization was divided in two major steps:

- Parametric studies for optimization, which were conducted for each element (parameters) of the antenna and determine the effect on their characteristics.
- Particle swarm optimization (PSO), which was used accordingly to enhance the desired antenna characteristics after identifying critical parameters from the parametric studies.

In this way, a compromise between parameters and characteristics was calculated and the best parameter goal for the antenna optimization was achieved.

2.2 Simulation results with Taconic TLX substrate

This section presents the results obtained from the first antenna design with referral parameters from the literature shown in Table 2.1 for dielectric substrate Taconic TLX of thickness h = 3 mm, relative permittivity ε_r = 2.55 and loss tangent tgδ = 0.0019 analyzed for a 5.5 - 7 GHz frequency band.

Figure 2.10 shows the simulated reflection coefficient of the investigated antenna. It can be observed that two resonant frequencies are present, the lower resonant frequency at 5.86 GHz equal to -19.4 dB and the higher resonant frequency at 6.72 GHz equal to -15.2 dB. Moreover, an impedance bandwidth of 19.9% for $|S_{11}| < -10$ dB from 5.66 GHz to 6.91 GHz. In addition to this, a similar trend can be seen with the reflection coefficient presented in the literature.

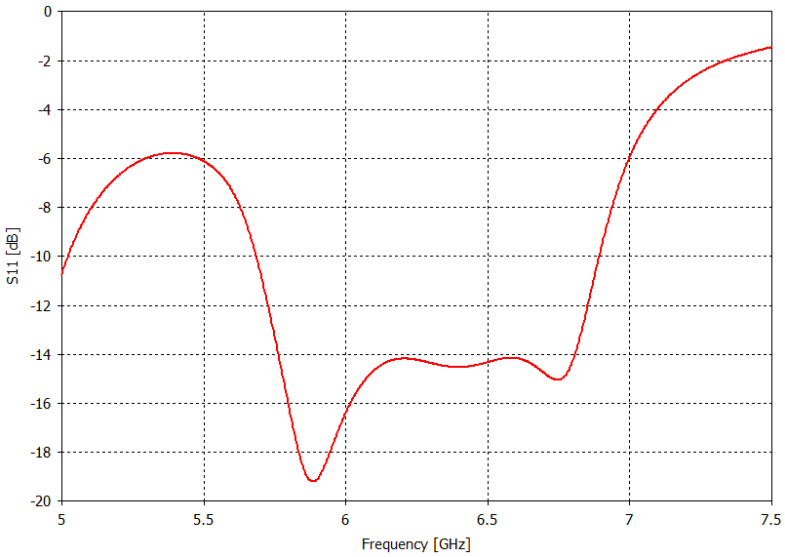

Figure 2.10 Reflection coefficient of the antenna with Taconic TLX substrate.

Figures 2.11 - 2.13 present the directivity characteristics in H and E planes at 5.9 GHz, 6.3 GHz and 6.6 GHz, respectively. The same frequencies analyzed in the literature were taken to verify the radiation patterns of the antenna. In Figure 2.13 the maximum gain (peak gain) at 6.6 GHz in the main lobe direction is depicted. The simulated peak gain is equal to 9.32 dBi and the elevation angle θ is equal to 23°. The side lobe level is -15.5 dB.

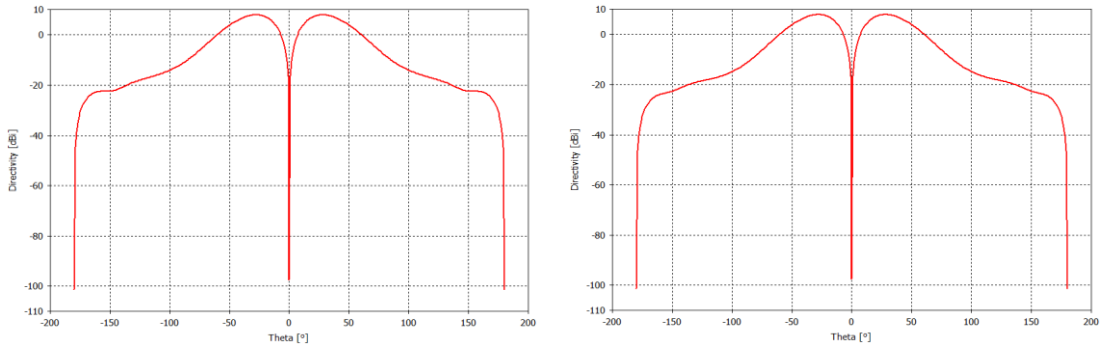

a) b)

Figure 2.11 Directivity with Taconic TLX substrate at 5.9 GHz – a) H-plane, b) E-plane.

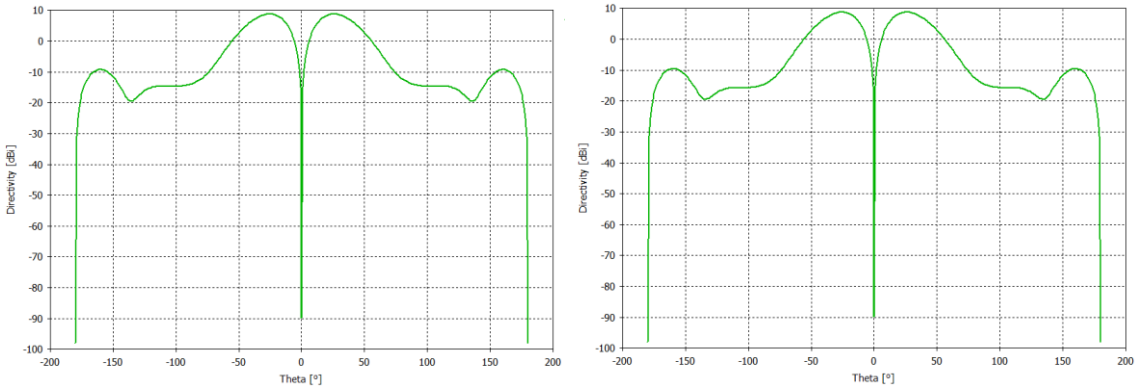

a) b)

Figure 2.12 Directivity with Taconic TLX substrate at 6.3 GHz – a) H-plane, b) E-plane.

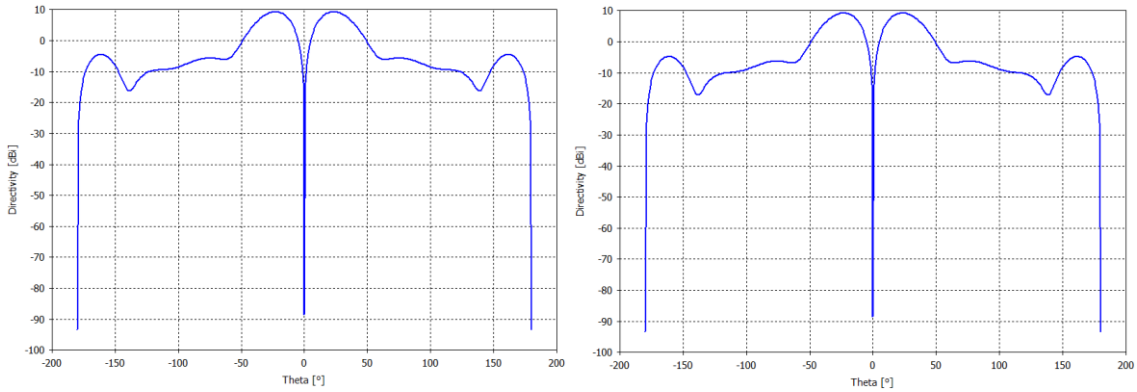

a) b)

Figure 2.13 Directivity with Taconic TLX substrate at 6.6 GHz – a) H-plane, b) E-plane.

The radiation patterns in 3D view at 6.6 GHz are shown in Figure 2.14. The graph reveals that the investigated antenna owns a wide conical-beam radiation above its surface corresponding to a dipole antenna and moreover, a highlighted circular polarization. Both conical-beam radiation characteristics are produced by the slot patches and perturbation elements in the antenna design, respectively, as explained in Section 2.1.2.

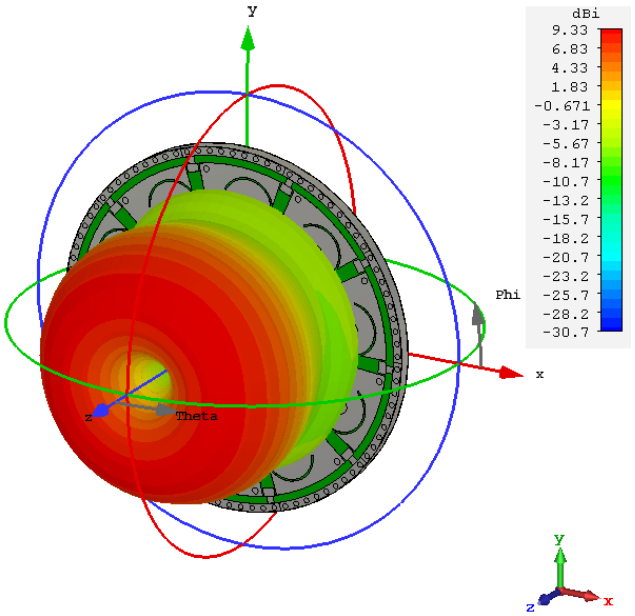

Figure 2.14 Radiation patterns in 3D view with Taconic TLX substrate at 6.6 GHz.

As the axial ratio describes the polarization of an antenna, for CP antennas this parameter should be less than 3 dB whereas the realized gain of an antenna does not include reflection losses. The simulated results of both parameters, respectively, can be observed in Figure 2.15. The axial ratio bandwidth is equal to 13.2 % for AR < 3 dB from 5.82 GHz to 6.64 GHz. The minimum AR equal to 1.2 dB is obtained at 6.1 GHz. In addition to this, the realized gain of the antenna is 8.9 dB at 6.6 GHz. Both parameters were simulated in the main lobe direction of the antenna $\theta = 23°$, previously depicted in the directivity patterns.

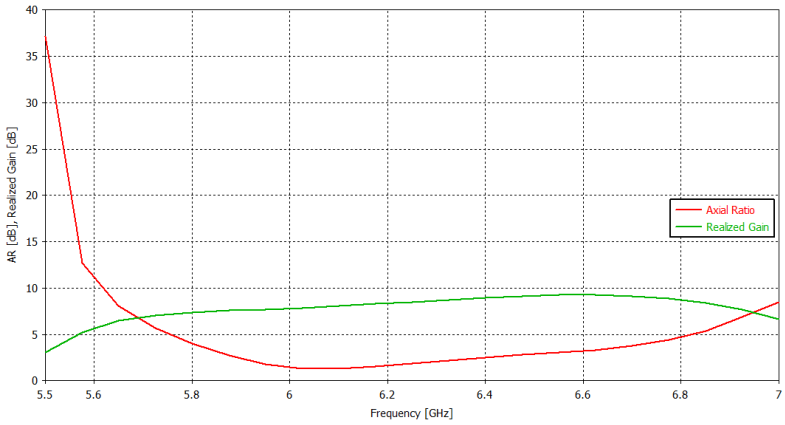

Figure 2.15 Axial ratio and realized gain with Taconic TLX substrate.

2.2.1 Verification of simulated results with published results in the literature

Table 2.2 summarizes the results obtained in the simulations and makes a comparison with the measured results published in the primary literature of this work. In the published results, a measured impedance bandwidth of 20.4% (5.54 GHz - 6.8 GHz) for $|S_{11}| < -10$ dB is exhibited. Moreover, an axial ratio bandwidth of 17% (5.65 GHz - 6.7 GHz) for AR < 3 dB, and a RCHP peak gain of 8.25 dBi at 6.15 GHz are presented. According to the literature, these results were measured in the main lobe direction at $\theta = 28°$ and $\varphi = 0°$.

Table 2.2 Comparison of simulated results and published results in the literature [1].

	Frequency [GHz]	Impedance bandwidth [%]	AR bandwidth [%]	Peak gain [dBi]
Literature (measured)	6.15	20.4	17	8.25
This work (simulated)	6.6	19.7	13.2	9.32

The results presented in these sections highlight a good agreement between the measured results in the literature and the simulated results of the designed antenna in the present work, as well as the overall behavior of its characteristics previously depicted.

2.3 Simulation results with Arlon CuClad 217 substrate

In the first stage of the present work, Arlon CuClad 217 substrate was assigned to be used in two taped pieces of thickness h =1.524 mm for the fabrication of the antenna. However, it was not possible to fabricate the antenna in this way because the workshop technology did not support the elaboration of such amount of vias with taped substrates in this antenna model. Hence, a new suitable substrate should be chosen for realization. The analysis and optimization results of antenna with the first substrate are presented in the following sections.

Simulations were performed for a 5.5 - 7 GHz frequency band with the following properties of the substrate: thickness h = 3.048 mm, relative permittivity ε_r = 2.17 and loss tangent tgδ = 0.0009.

2.3.1 Analysis with referral parameters

This section deals with the antenna analysis using referral parameters from the literature to examine the initial behavior of the characteristics and evaluate their subsequent optimization in terms of S_{11}, AR and gain.

The simulated reflection coefficient is shown in Figure 2.16. It can be noted that the resonant frequencies are shifted to the right of the operating band. This effect is produced by the relative permittivity of the substrate, which is lower than the permittivity of the substrate utilized in the literature (See Section 1.2.4.1). The lower resonant frequency is at 6.48 GHz equal to -30.5 dB and the higher resonant frequency at 6.99 GHz equal to -

41.4 dB. The impedance bandwidth is 17.4% for $|S_{11}| < -10$ dB from 6.05 GHz to 7.2 GHz.

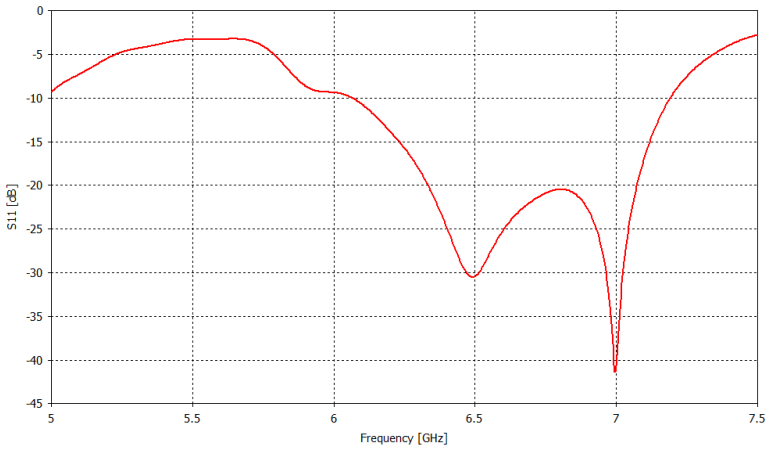

Figure 2.16 Reflection coefficient of the antenna with Arlon CuClad 217 substrate.

Figures 2.17 - 2.19 show the directivity characteristics in H and E planes at 6.1 GHz, 6.5 GHz and 6.9 GHz, respectively. Figure 2.13 depicts the peak gain at 6.9 GHz equal to 9.64 dBi in the main lobe direction equal to 22°, side lobe level -14.7 dB. Hence, this characteristic is not affected overall by the new substrate properties.

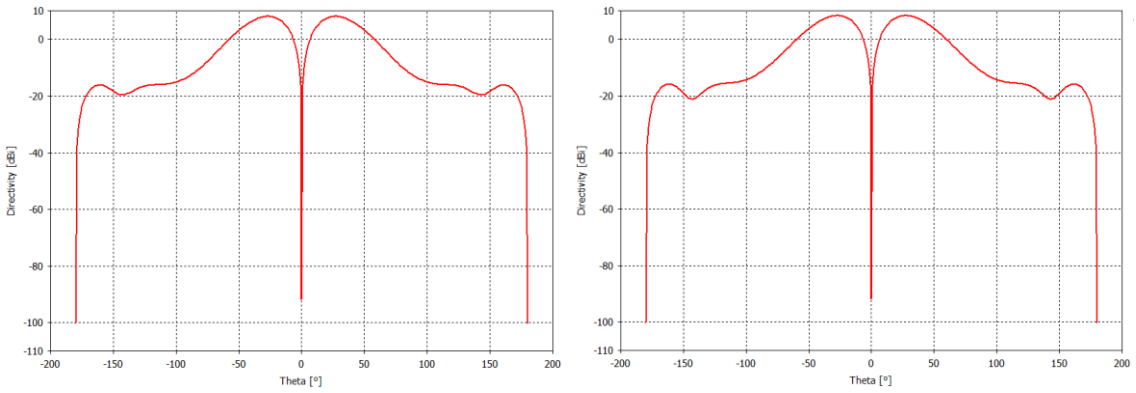

a) b)

Figure 2.17 Directivity with Arlon CuClad 217 substrate at 6.1 GHz – a) H-plane, b) E-plane.

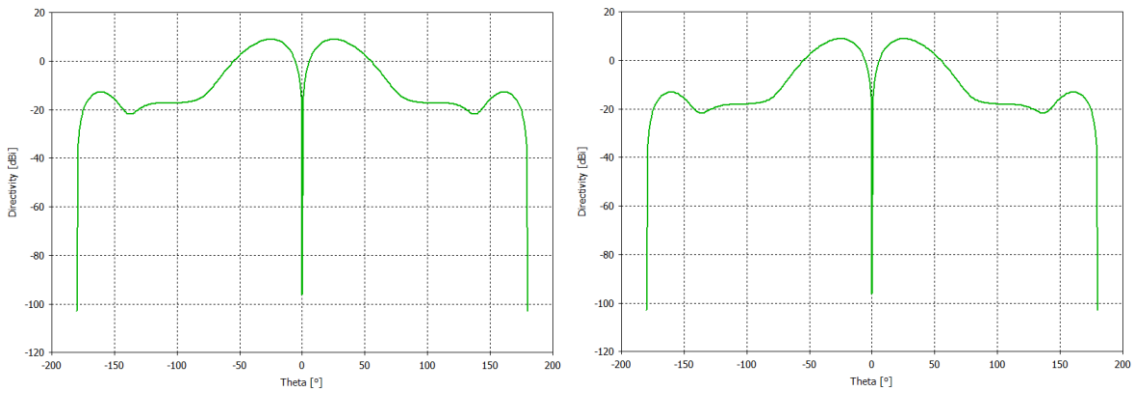

a) b)

Figure 2.18 Directivity with Arlon CuClad 217 substrate at 6.5 GHz – a) H-plane, b) E-plane.

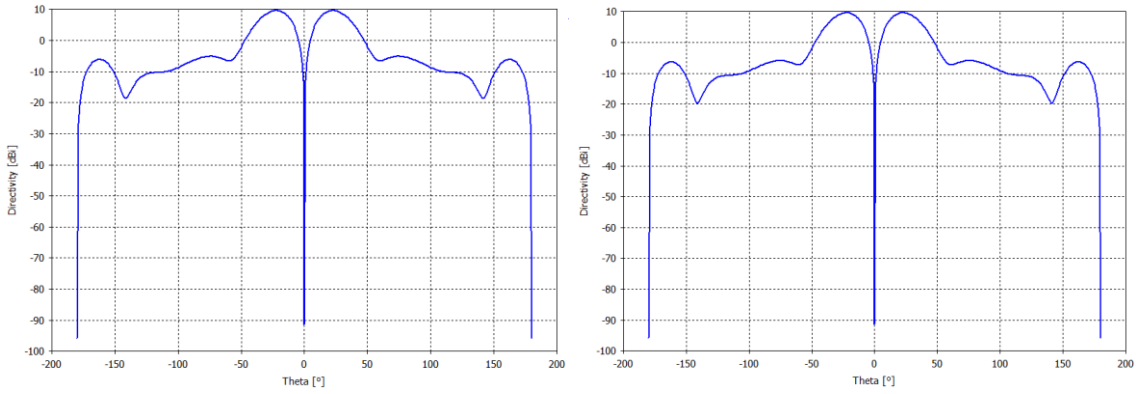

a) b)

Figure 2.19 Directivity with Arlon CuClad 217 substrate at 6.9 GHz – a) H-plane, b) E-plane.

The axial ratio and the realized gain are depicted in Figure 2.20. Both quantities were analyzed in the main lobe direction of the antenna θ=22°, previously depicted in the directivity patterns. The axial ratio bandwidth is equal to 11% for AR < 3 from 6.1 GHz to 6.88 GHz. The minimum AR equal to 0.5 dB is obtained at 6.35 GHz. Moreover, the realized gain of the antenna is equal to 9.6 dB at 6.9 GHz. These obtained results reveal that the axial ratio and the gain of the antenna are not considerably affected by the new substrate as well.

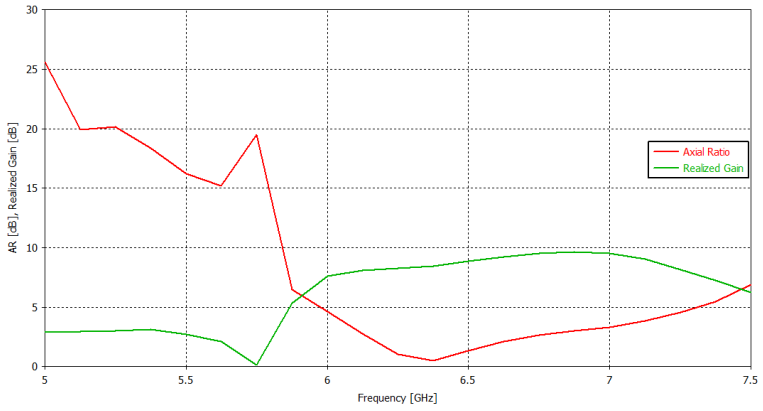

Figure 2.20 Axial ratio and realized gain with Arlon CuClad 217 substrate.

2.3.2 Parametric studies for optimization

This section is focused on the parametric analysis performed for all the parameters of the investigated antenna and their effect on basic characteristics. The aim of this analysis is to find the critical parameters for a suitable optimization.

Figures 2.21 - 2.31 show the simulated parameter sweeps performed for following parameters referred before in Table 2.1: S_1, S_2, S_3, R_5, R_6, R_g, d_1, d_2, d_3, D_1 *and* D_2. The reflection coefficient, axial ratio and realized gain results are presented.

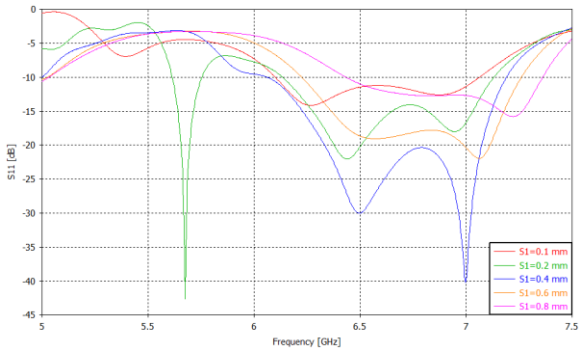

a)

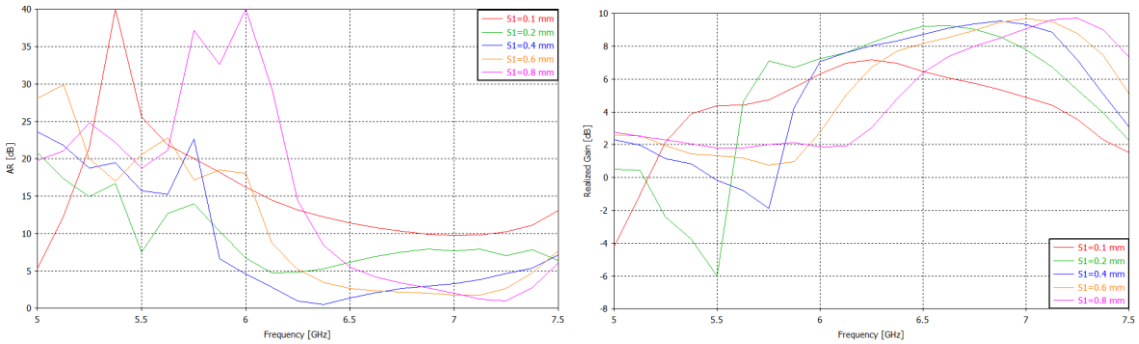

b) c)

Figure 2.21 Parametric analysis for S_1 parameter with Arlon CuClad 217 substrate – a) Reflection coefficient, b) Axial ratio, c) Realized gain.

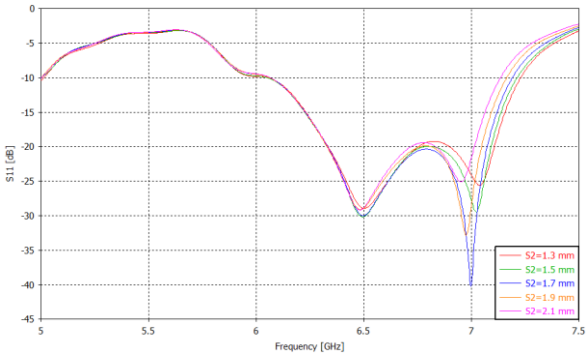

a)

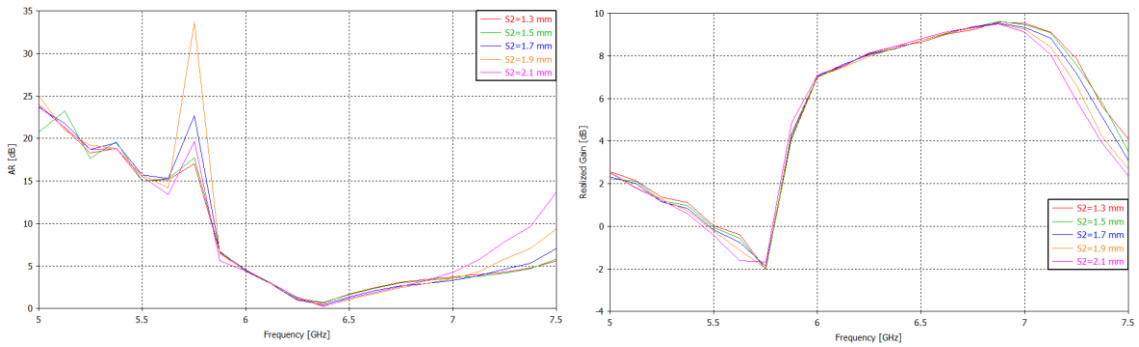

b) c)

Figure 2.22 Parametric analysis for S_2 parameter with Arlon CuClad 217 substrate – a) Reflection coefficient, b) Axial ratio, c) Realized gain.

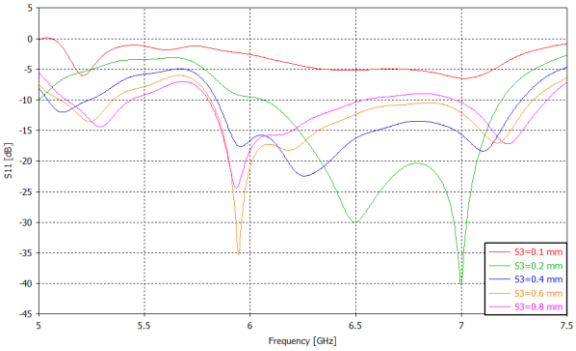

a)

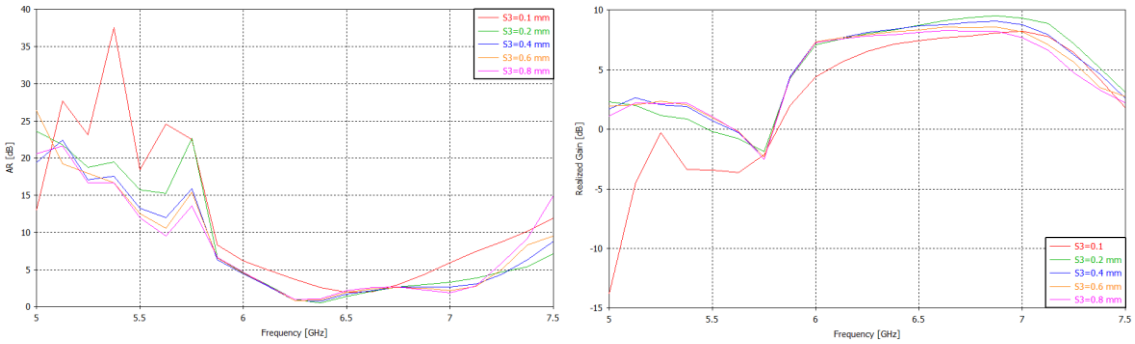

b) c)

Figure 2.23 Parametric analysis for S_3 parameter with Arlon CuClad 217 substrate – a) Reflection coefficient, b) Axial ratio, c) Realized gain.

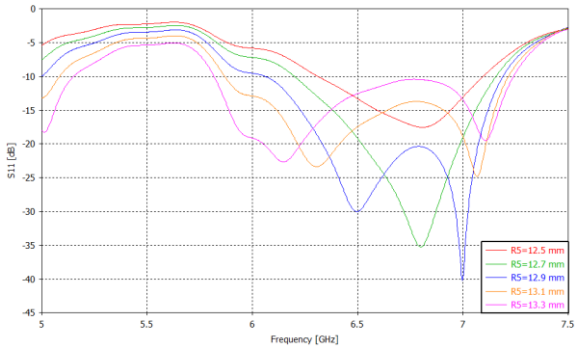

a)

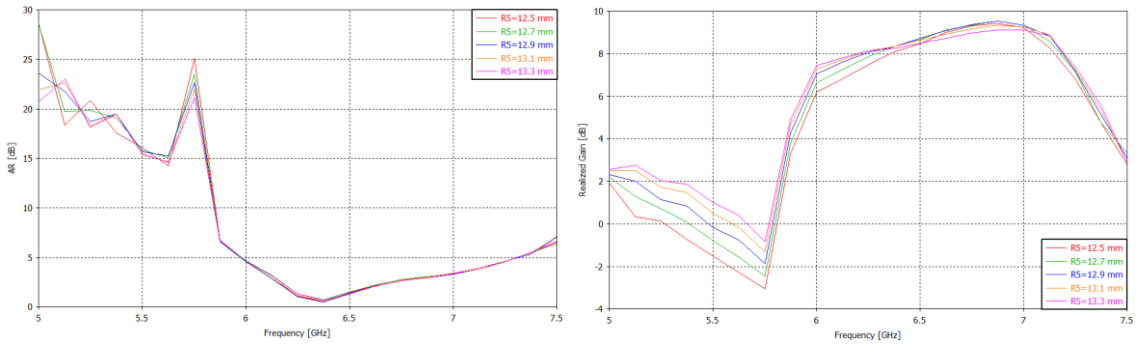

b) c)

Figure 2.24 Parametric analysis for R_5 parameter with Arlon CuClad 217 substrate – a) Reflection coefficient, b) Axial ratio, c) Realized gain.

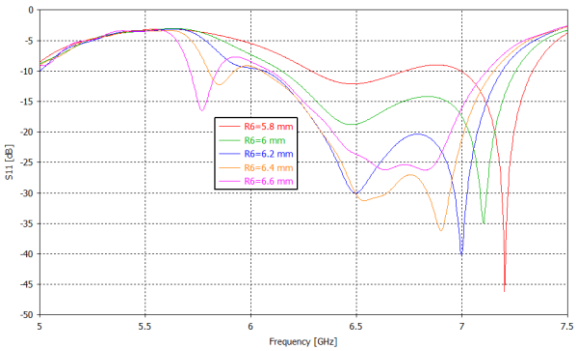

a)

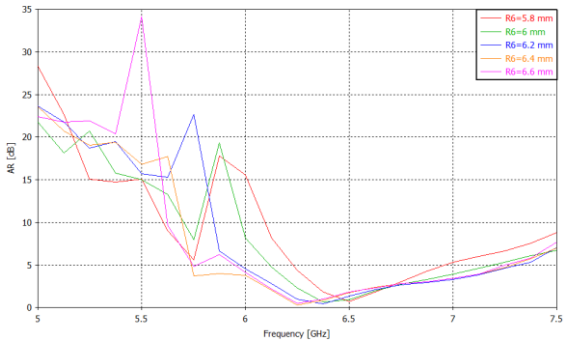

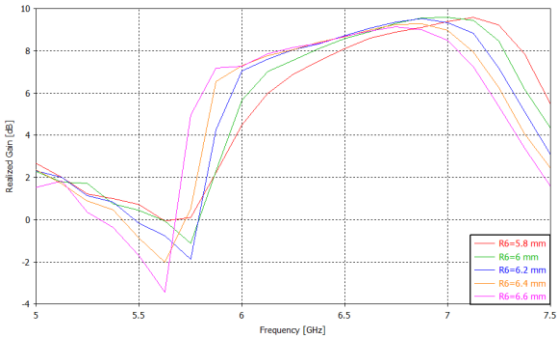

b) c)

Figure 2.25 Parametric analysis for R_6 parameter with Arlon CuClad 217 substrate – a) Reflection coefficient, b) Axial ratio, c) Realized gain.

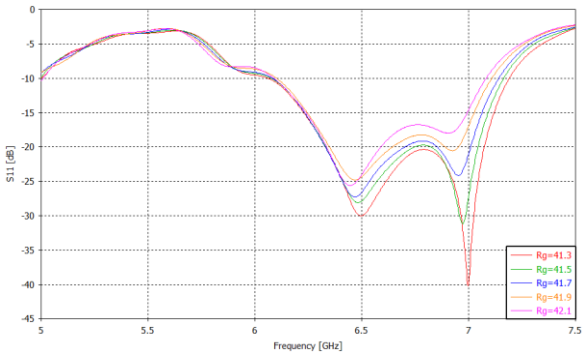

a)

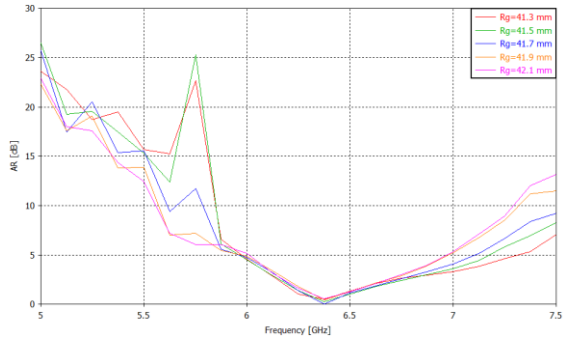

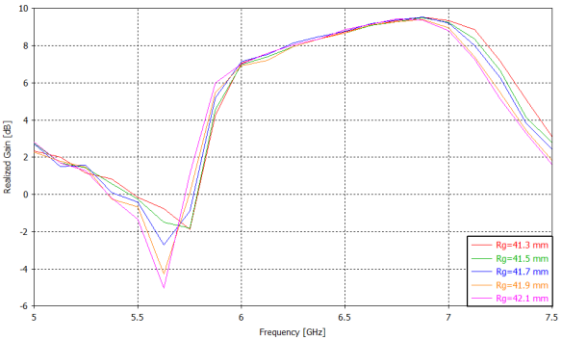

b) c)

Figure 2.26 Parametric analysis for R_g parameter with Arlon CuClad 217 substrate – a) Reflection coefficient, b) Axial ratio, c) Realized gain.

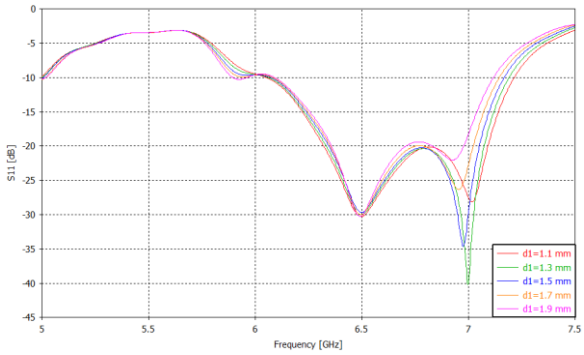

a)

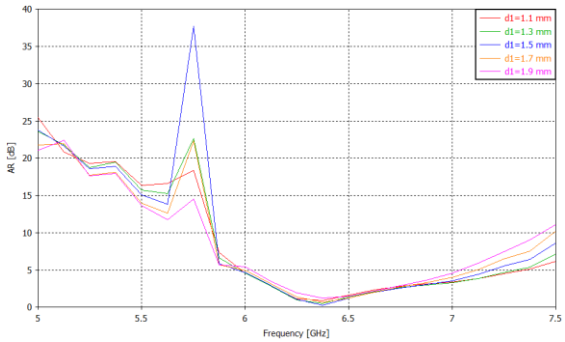

b)

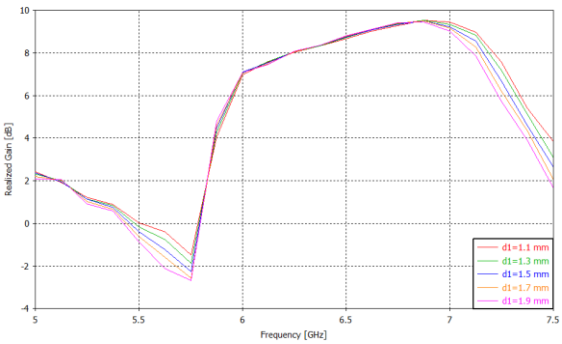

c)

Figure 2.27 Parametric analysis for d_1 parameter with Arlon CuClad 217 substrate – a) Reflection coefficient, b) Axial ratio, c) Realized gain.

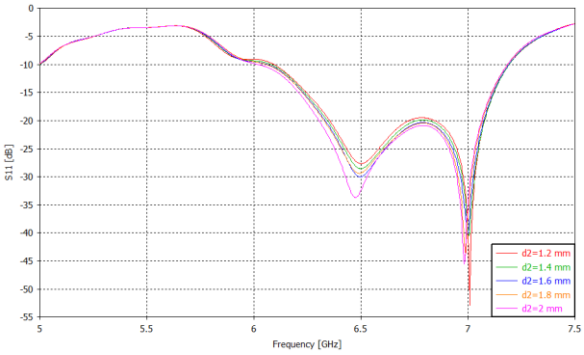

a)

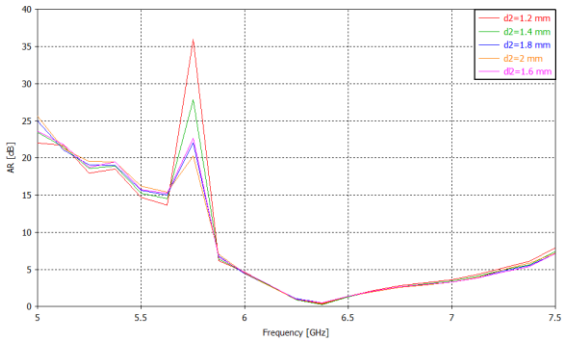

b)

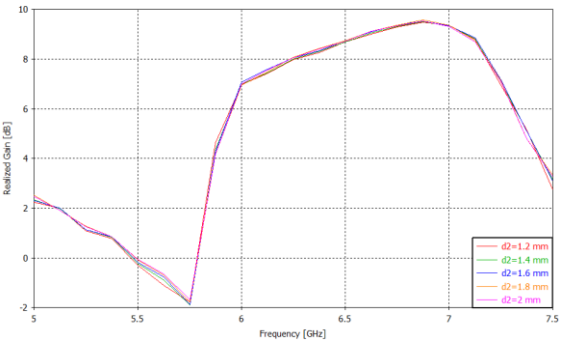

c)

Figure 2.28 Parametric analysis for d_2 parameter with Arlon CuClad 217 substrate – a) Reflection coefficient, b) Axial ratio, c) Realized gain.

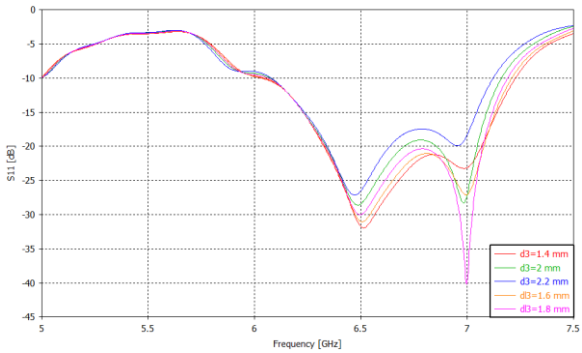

a)

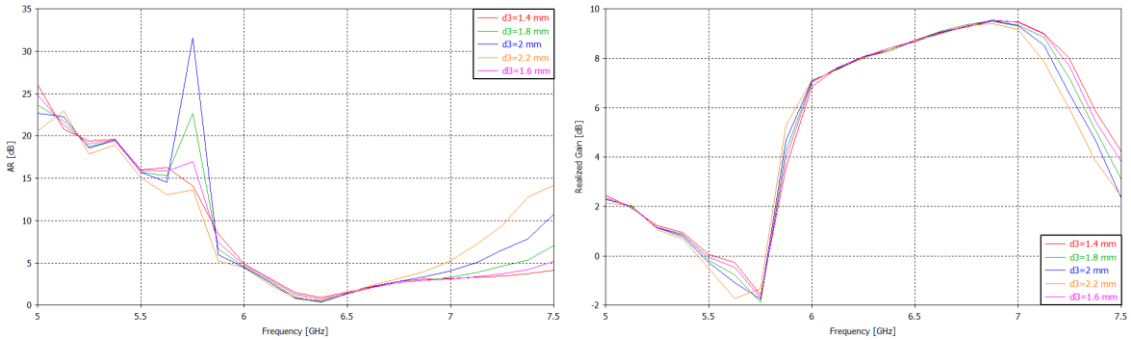

b) c)

Figure 2.29 Parametric analysis for d_3 parameter with Arlon CuClad 217 substrate – a) Reflection coefficient, b) Axial ratio, c) Realized gain.

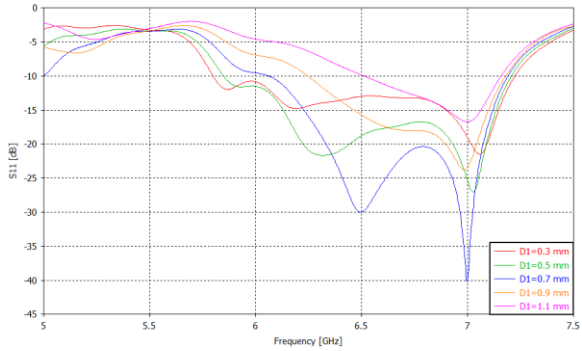

a)

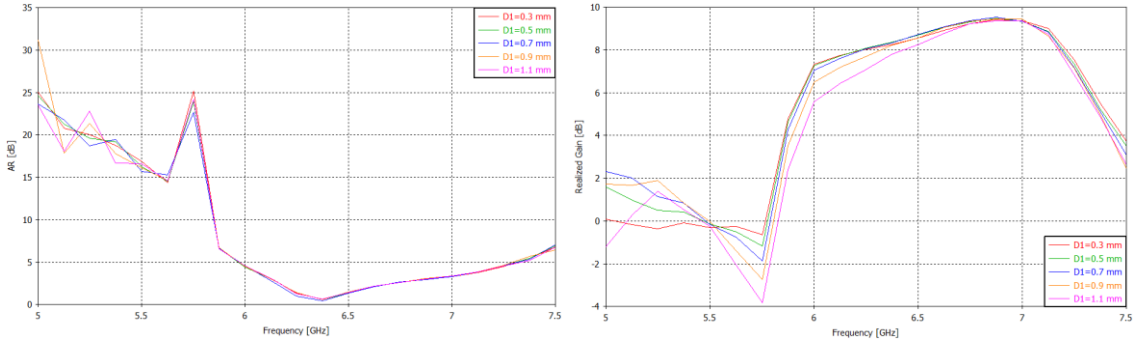

b) c)

Figure 2.30 Parametric analysis for D_1 parameter with Arlon CuClad 217 substrate – a) Reflection coefficient, b) Axial ratio, c) Realized gain.

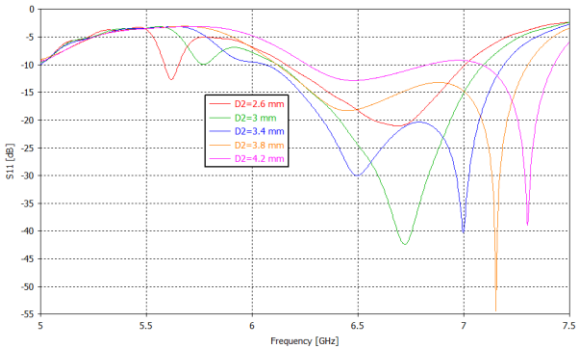

a)

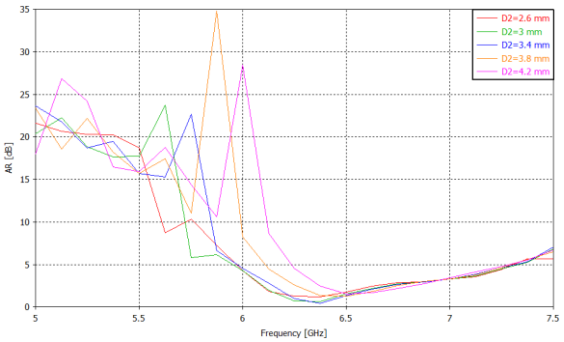

b)

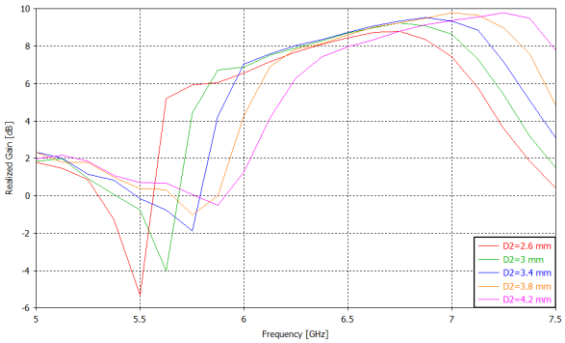

c)

Figure 2.31 Parametric analysis for D_2 parameter with Arlon CuClad 217 substrate – a) Reflection coefficient, b) Axial ratio, c) Realized gain.

As shown in the graphs above, characteristics vary notably with respect to some parameters. These sensitive parameters in the antenna, the so called critical parameters to be optimized, are presented in Table 2.3.

Table 2.3 Critical parameters and their effect on the antenna characteristics.

Parameter	Description	Affected characteristic
S_1	Width of annular ring element	S_{11}: Same effect on both resonant frequencies
		AR: Yes, Gain: Yes
S_3	Width of outer circular sector on the monopole	S_{11}: Same effect on both resonant frequencies
		AR: No, Gain: No
R_5	Radius up to internal via of the monopole	S_{11}: Bigger effect in lower resonant frequency than higher one.
		AR: No, Gain: No
R_6	Radius of shorted annular ring slot	S_{11}: Same effect on both resonant frequencies
		AR: Yes, Gain: Yes
D_1	Diameter of internal via of the monopole	S_{11}: Bigger effect in lower resonant frequency than higher one.
		AR: No, Gain: No
D_2	Diameter of internal via of the shorted annular ring slot	S_{11}: Bigger effect in higher resonant frequency than lower one.
		AR: Yes, Gain: Yes

2.3.3 Particle swarm optimization

The particle swarm optimizer (POS) is a powerful global optimizer, which is based on an algorithm that treats points in parameter space as moving particles. At each iteration, the positions of the particles changes, not only according to the position of each particle, but the best position of the swarm as well [12]. Particle swarm optimization is suitable for models with many parameters as the investigated antenna.

Figure 2.32 shows the settings, goals and results information in the particle swarm optimizer. The critical parameters, previously analyzed in the parametric studies, were defined in value ranges which represented a compromise between S_{11}, AR and gain for a good antenna performance. Non-critical parameters were left unchanged, as shown in Figure 2.32 a). Moreover, the definition of the goals can be observed in Figure 2.32 b), where S_{11} was set as the minimum possible value (-120 dB) in a range of 6 GHz - 6.5 GHz for a center frequency band tuning of both resonant frequencies (higher and lower) in the 5.5 GHz -7 GHz frequency band, AR was set to 0 dB to ensure the circular polarization in the antenna, and the realized gain was set to a high arbitrary magnitude never reached in previous simulations (12 dB) to attain the highest possible gain. Furthermore, all parameters were defined with a weight of 1, which indicates the high priority of the parameters to be optimized, and also establishes a compromise between them for the calculation. Finally, the optimized parameters results and simulation solver information are summarized in Figure 2.3.2 c).

	Parameter	Min	Max
☒	D1	0.3	0.9
☒	D2	2.4	3.4
☐	phi1	13.5	16.5
☐	phi2	27.54	33.66
☐	phi3	9.9	12.1
☐	phi4	36	44
☐	phi5	5.4	6.6
☒	R5	12.8	13.3
☒	R6	5.8	6.6
☐	Rg	37.17	45.43
☐	ri	0.54	0.66
☐	ro	1.809	2.211
☒	S1	0.2	0.6
☐	S2	1.53	1.87
☒	S3	0.15	0.6
☐	S4	0.315	0.385
☐	t	0.0153	0.0187
☐	ts	2.862	3.498

a)

	ID	Type	Operator	Target	Range	Weight
☒	0	1DC: .\S-Parameters\S1,1	min	-120	6...6.5	1.0
☒	1	TBPP 1D: Axial Ratio	=	0	5.5...7	1.0
☒	2	TBPP 1D: Realized Gain	=	12	5.5...7	1.0

b)

```
Algorithm: Particle Swarm Optimization
145 of maximal 145 solver runs done

Number of evaluations: 145
              (solver: 145)
First goal function value   = 155.9337617
Best goal function value    = 140.366026215
Last goal function value    = 140.366026215

Best parameters so far:

 D1 = 0.68609
 D2 = 2.81886
 R5 = 13.1573
 R6 = 5.97226
 S1 = 0.336454
 S3 = 0.540319
```

c)

Figure 2.32 Particle swarm optimization with Arlon CuClad 217 substrate – a) Critical parameters definition, b) Goals definition, c) Optimized parameters results.

Figure 2.33 presents the antenna characteristics after the optimization procedure. In Figure 2.33 a) the reflection coefficient, the axial ratio, and the realized gain are depicted. The S_{11} parameter shows a better tuning in the operating frequency band with the lower resonant frequency at 5.72 GHz equal to -19.4 dB and the higher resonant frequency at 6.58 GHz equal to -19.7 dB. The impedance bandwidth is 23% for $|S_{11}| < -10$ dB from 5.38 GHz to 6.78 GHz whereas Figure 2.33 b) indicates the obtained axial ratio bandwidth equal to 19.4% for AR < 3 from 5.56 GHz to 6.76 GHz. The minimum AR equal to 0.3

dB is obtained at 5.88 GHz. In addition to this, the realized gain of the antenna is equal to 9.5 dB at 6.38 GHz. Both parameters were simulated in the main lobe direction with an elevation θ =23°.

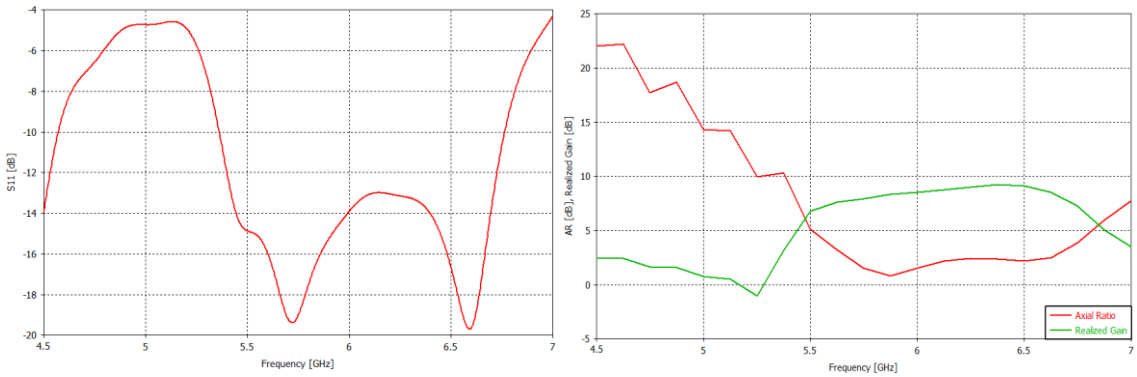

a) b)

Figure 2.33 Optimized characteristics with Arlon CuClad 217 substrate – a) Reflection coefficient b) Axial ratio and realized gain.

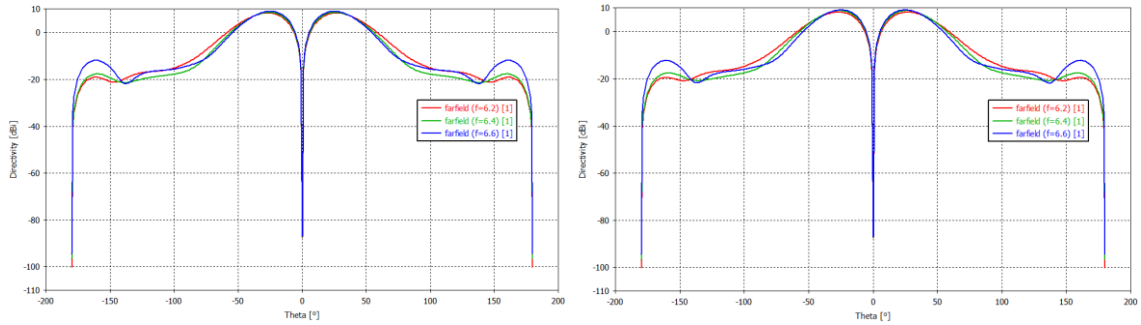

a) b)

Figure 2.34 Optimized directivity characteristics with Arlon CuClad 217 substrate at 6.2 GHz, 6.4 GHz, 6.6 GHz in the – a) H-plane, b) E-plane.

Optimized directivity patterns in the H and E planes at 6.2 GHz, 6.4 GHz and 6.6 GHz, respectively, are shown Figure 2.34. The maximum gain at 6.4 GHz in the main lobe direction is depicted. The obtained peak gain is equal to 9.72 dBi and the elevation angle θ is equal to 23°. The side lobe level is -15 dB.

Table 2.4 summarizes the results obtained with referral and optimized parameters of the antenna, in which is clearly noted an enhancement in the desired characteristics.

Table 2.4 Comparison of optimized and non-optimized characteristics with Arlon CuClad 217 substrate.

	Frequency [GHz]	Impedance bandwidth [%]	AR bandwidth [%]	Peak gain [dBi]
Referral parameters	6.9	17.4	11	9.64
Optimized parameters	6.4	23	19.4	9.72

2.4 Simulation results with Rogers 5870 substrate

As mentioned before in Section 2.3, a new substrate should be chosen for available fabrication technology in the workshop for this model. The main reason for the choice of the Rogers 5870 substrate was, firstly, its suitable relative permittivity, which is slightly lower than substrate utilized in the literature but not lower than Arlon, which effected a considerable frequency band shift before its optimization. This relative permittivity can allow good tuning and performance in the desired 5.5 GHz - 7 GHz operating frequency band. Secondly, it has similar thickness as the substrate in the literature, which overall exhibits a low profile prototype.

The properties of the Rogers 5870 considered for simulations are: thickness h = 3.18 mm, relative permittivity ε_r = 2.33 and loss tangent tgδ = 0.0012.

2.4.1 Analysis with referral parameters

In the same way as with Arlon substrate, this section is focused on the antenna analysis using referral parameters from the literature to examine the initial behavior of the characteristics for the optimization procedure.

The simulated reflection coefficient is depicted in Figure 2.35. It shows the lower resonant frequency at 6.28 GHz equal to -26.1 dB and the higher resonant frequency at 6.72 GHz equal to -32.7 dB. The impedance bandwidth is 15.9% for |S11| < -10 dB from 5.89 GHz to 6.91 GHz, which is properly tuned up in the desired frequency band.

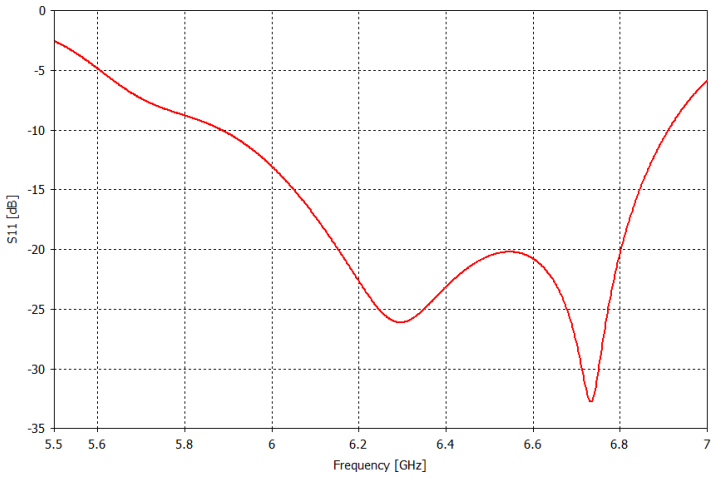

Figure 2.35 Reflection coefficient of the antenna with Rogers 5870 substrate.

Figures 2.36 - 2.38 shows the directivity characteristics simulated in the H and E planes at 6.1 GHz, 6.4 GHz and 6.7 GHz, respectively. Figure 2.38 depicts the peak gain at 6.7 GHz equal to 9.42 dBi in the main lobe direction equal to 23°, the side lobe level is -14.3 dB. From the graphs, it can be observed that, as well as with Arlon substrate, this characteristic is not affected by the substrate properties.

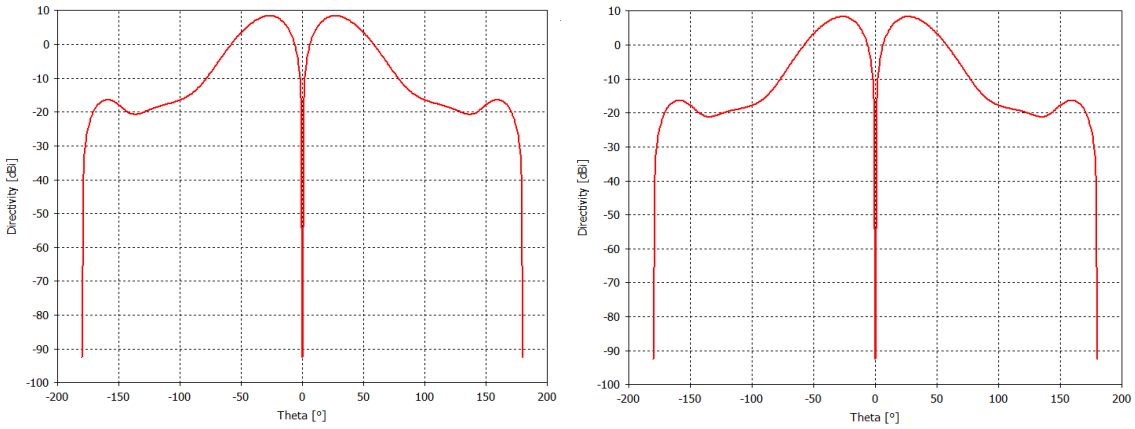

a) b)

Figure 2.36 Directivity with Rogers 5870 substrate at 6.1 GHz in the – a) H-plane, b) E-plane.

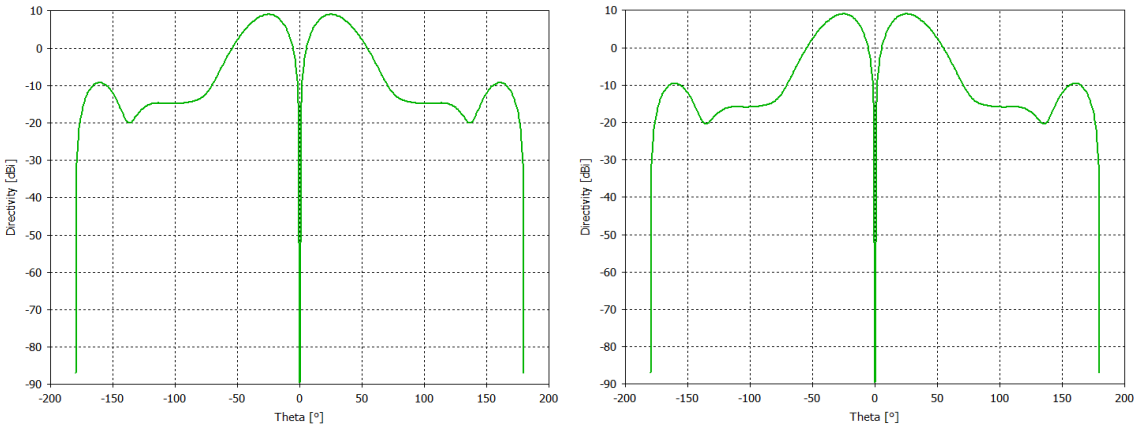

a) b)

Figure 2.37 Directivity with Rogers 5870 substrate at 6.4 GHz in the – a) H-plane, b) E-plane.

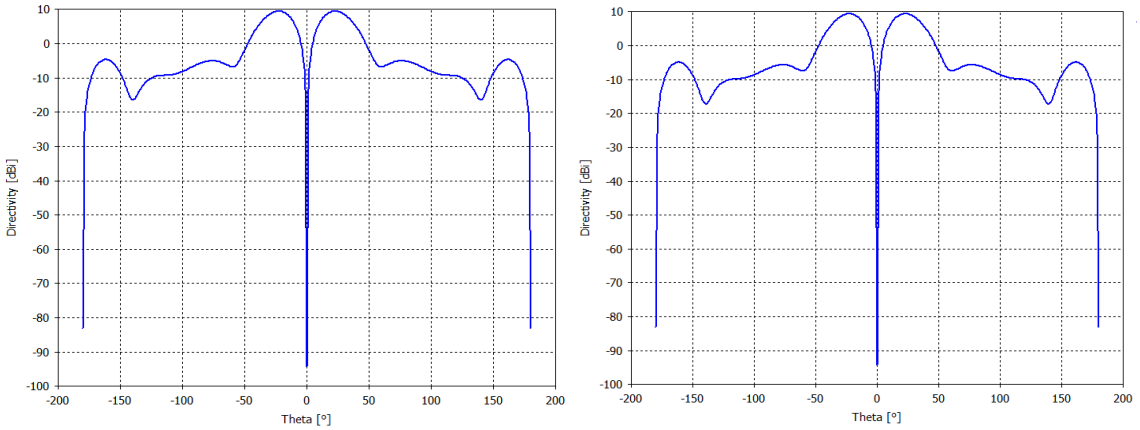

a) b)

Figure 2.38 Directivity with Rogers 5870 substrate at 6.7 GHz in the – a) H-plane, b) E-plane.

The axial ratio and the realized gain are presented in Figure 2.39. Both were simulated in the main lobe direction of the antenna θ =23°, previously showed in the directivity characteristics. The axial ratio bandwidth is equal to 15.5 % for AR < 3 from 5.91 GHz to 6.9 GHz. The minimum AR equal to 0.2 dB is obtained at 6.1 GHz. Furthermore, the realized gain of the antenna is equal to 9.3 dB at 6.7 GHz.

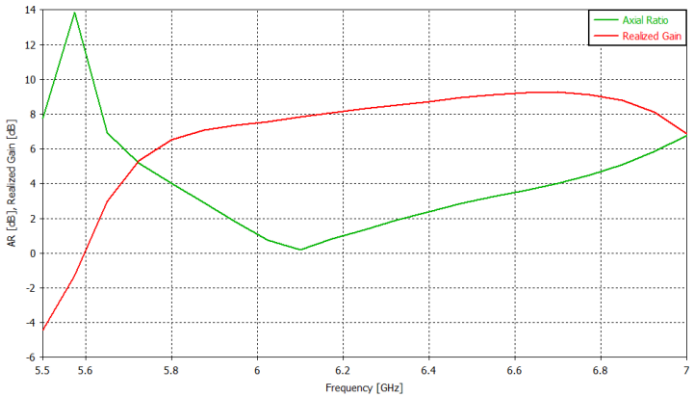

Figure 2.39 Axial ratio and realized gain with Rogers 5870 substrate.

2.4.2 Parametric studies for optimization

As stated as a part of the optimization of the antenna, Figures 2.40 - 2.50 show the parametric analysis for all antenna parameters listed in Table 2.1: S_1, S_2, S_3, R_5, R_6, R_9, d_1, d_2, d_3, D_1 *and* D_2. The reflection coefficient, axial ratio and realized gain results are presented.

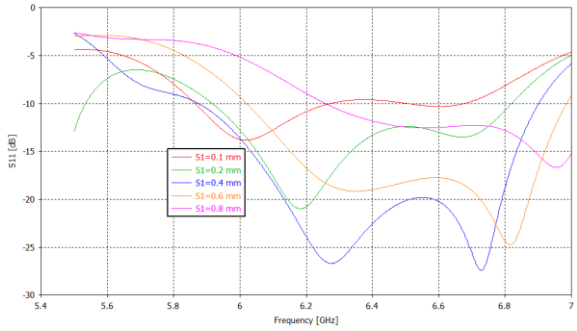

a)

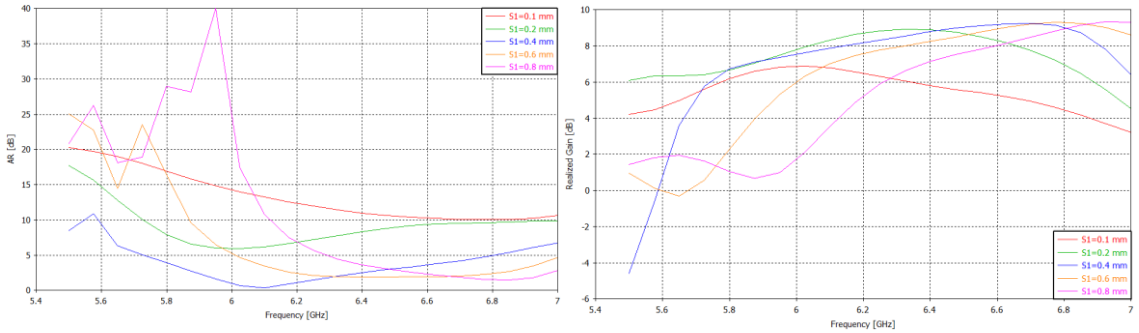

b) c)

Figure 2.40 Parametric analysis for S_1 parameter with Rogers 5870 substrate – a) Reflection coefficient, b) Axial ratio, c) Realized gain.

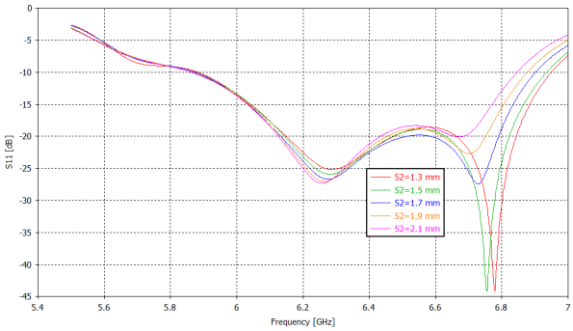

a)

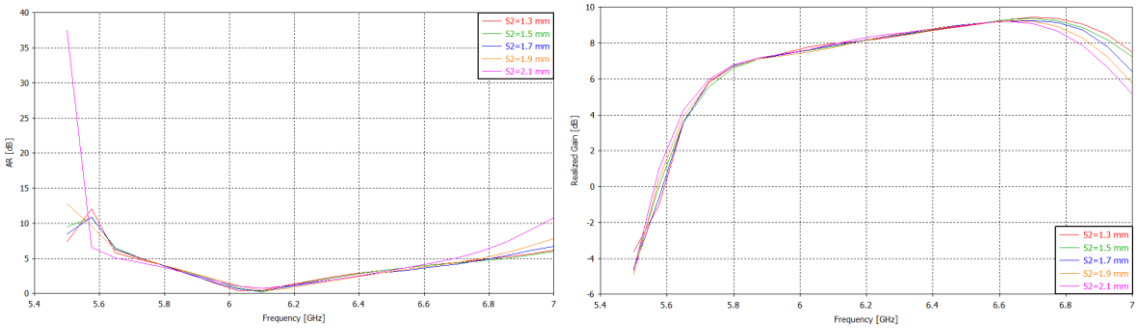

b) c)

Figure 2.41 Parametric analysis for S_2 parameter with Rogers 5870 substrate – a) Reflection coefficient, b) Axial ratio, c) Realized gain.

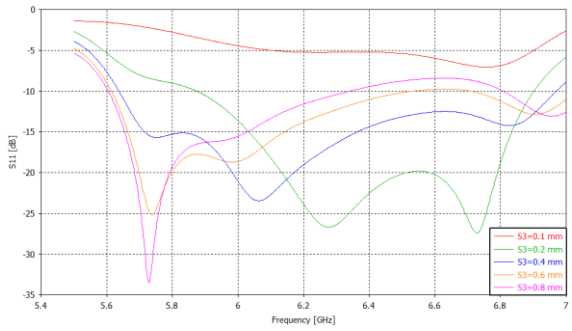

a)

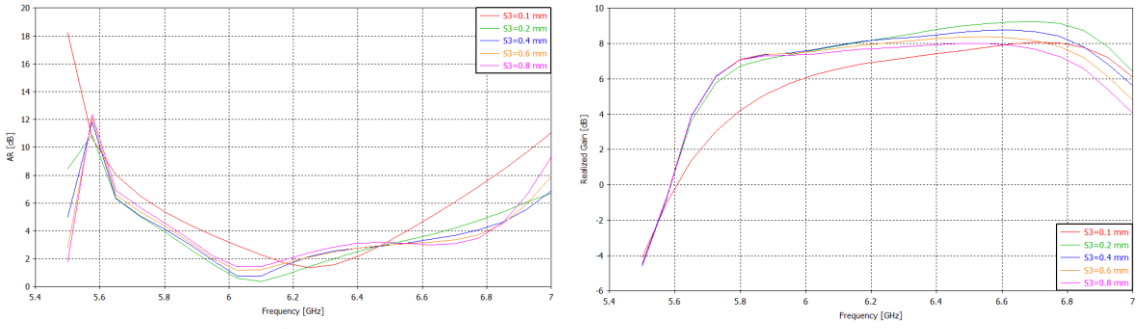

b) c)

Figure 2.42 Parametric analysis for S_3 parameter with Rogers 5870 substrate – a) Reflection coefficient, b) Axial ratio, c) Realized gain.

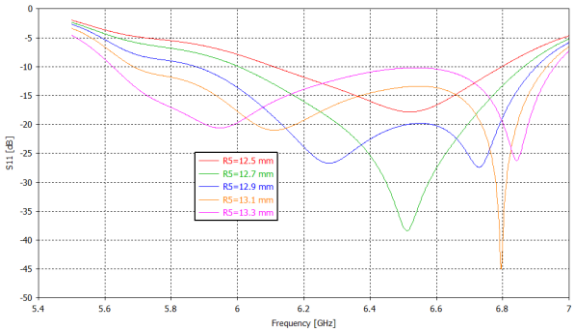

a)

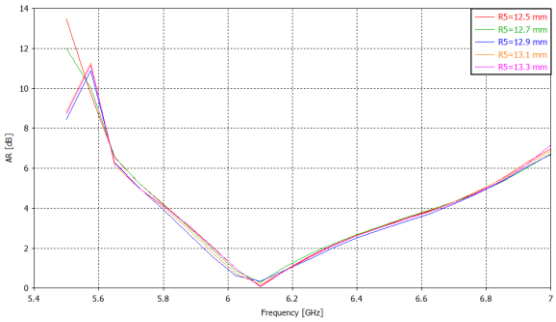

b)

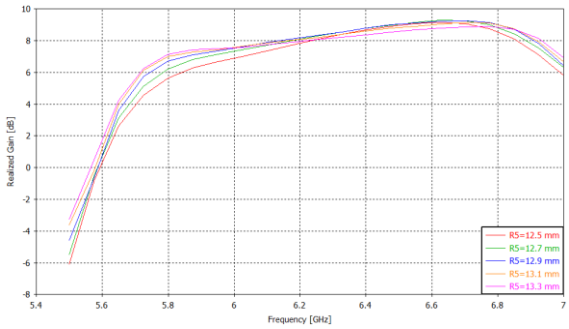

c)

Figure 2.43 Parametric analysis for R_5 parameter with Rogers 5870 substrate – a) Reflection coefficient, b) Axial ratio, c) Realized gain.

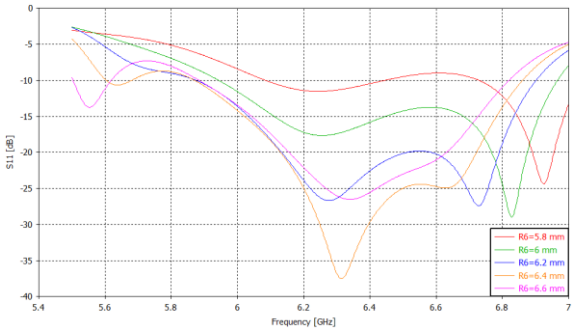

a)

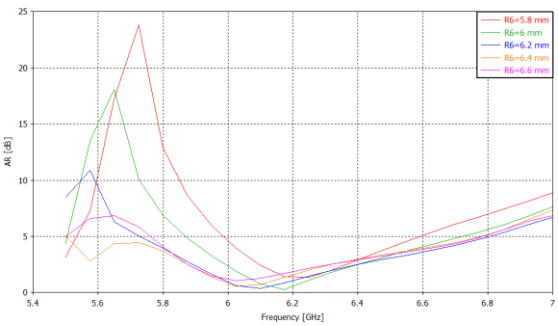

b)

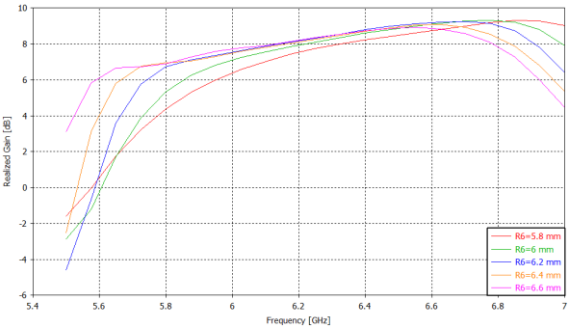

c)

Figure 2.44 Parametric analysis for R_6 parameter with Rogers 5870 substrate – a) Reflection coefficient, b) Axial ratio, c) Realized gain.

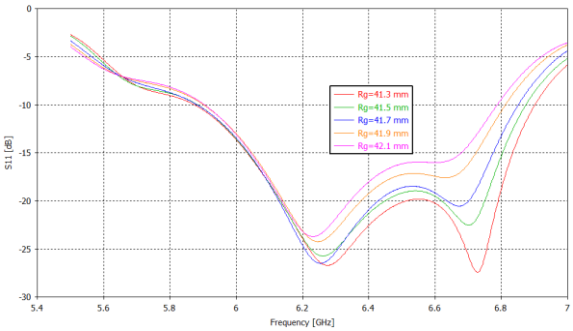

a)

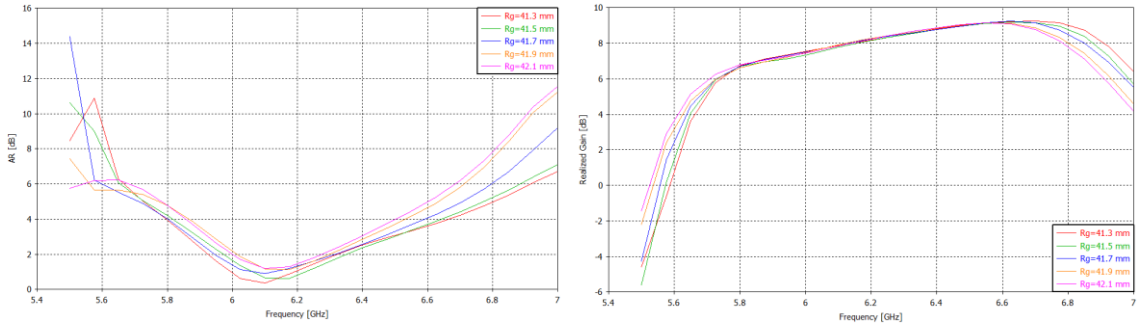

a) b)

Figure 2.45 Parametric analysis for R_g parameter with Rogers 5870 substrate – a) Reflection coefficient, b) Axial ratio, c) Realized gain.

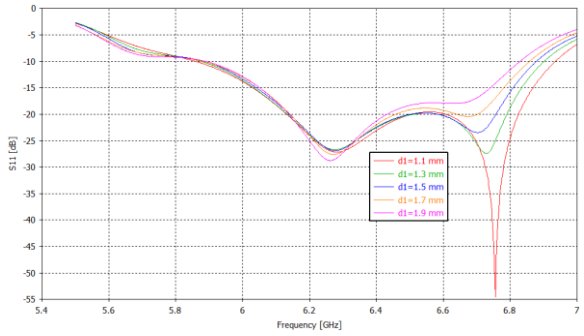

a)

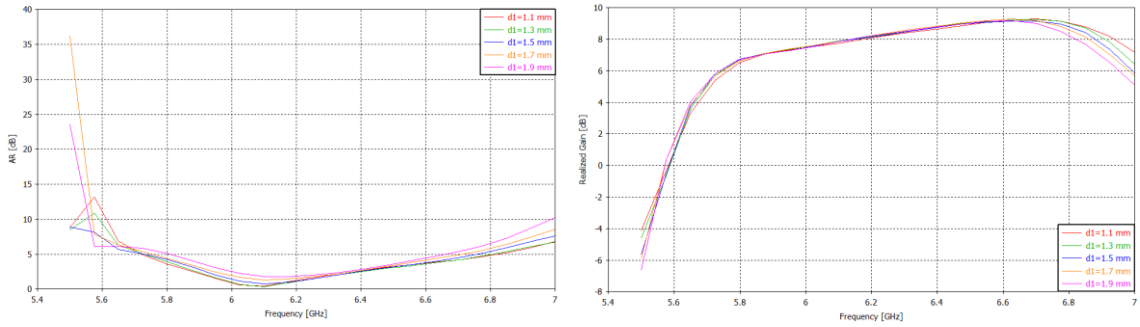

b) c)

Figure 2.46 Parametric analysis for d_1 parameter with Rogers 5870 substrate – a) Reflection coefficient, b) Axial ratio, c) Realized gain.

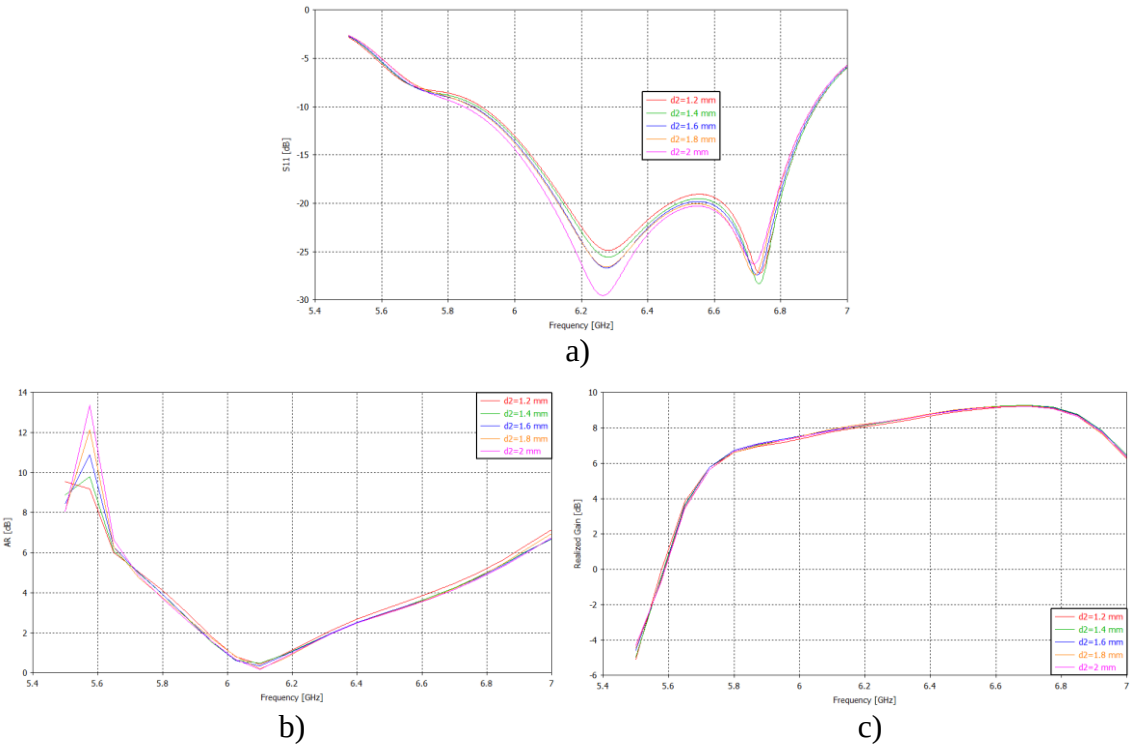

Figure 2.47 Parametric analysis for d_2 parameter with Rogers 5870 substrate – a) Reflection coefficient, b) Axial ratio, c) Realized gain.

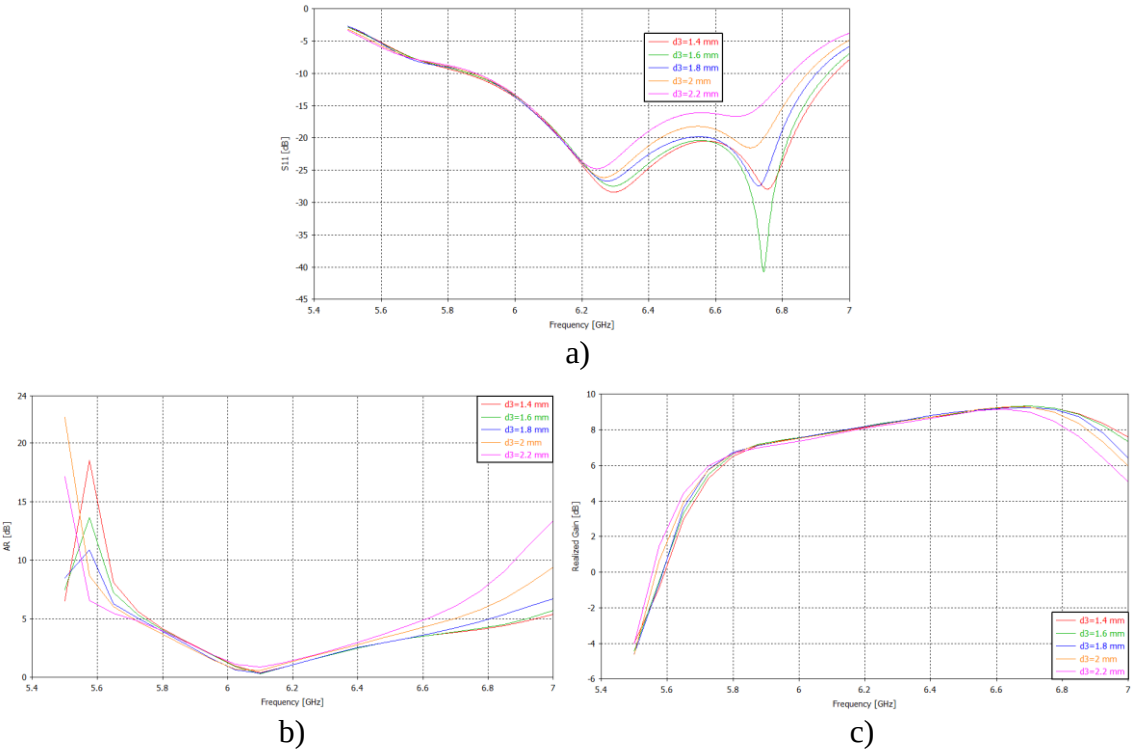

Figure 2.48 Parametric analysis for d_3 parameter with Rogers 5870 substrate – a) Reflection coefficient, b) Axial ratio, c) Realized gain.

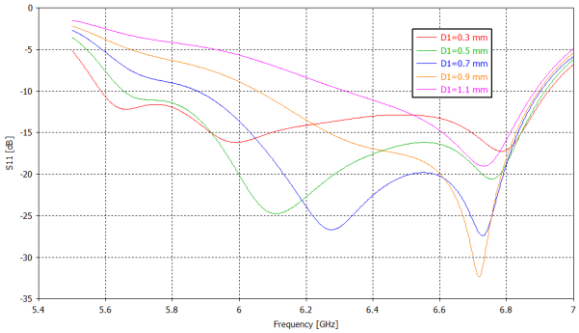

a)

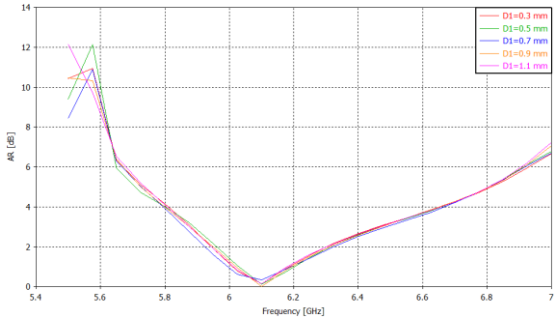

b)

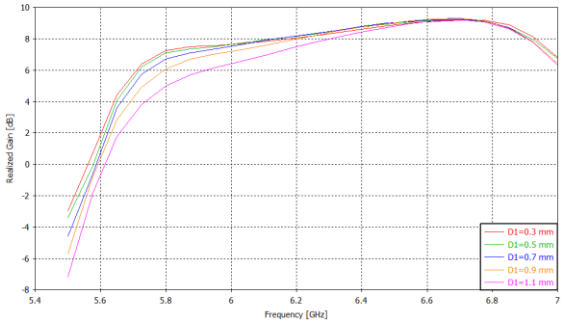

c)

Figure 2.49 Parametric analysis for D_1 parameter with Rogers 5870 substrate – a) Reflection coefficient, b) Axial ratio, c) Realized gain.

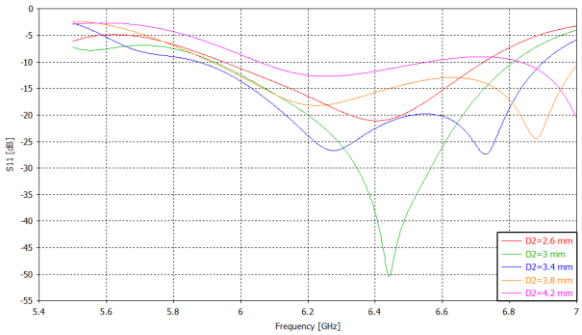

a)

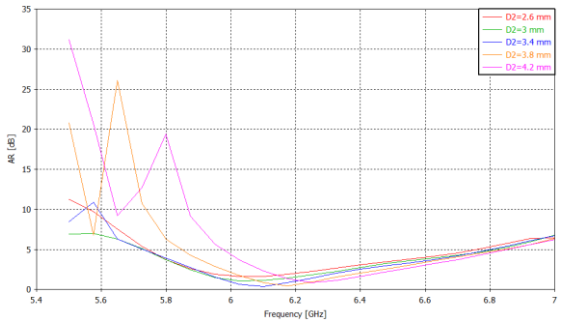

b)

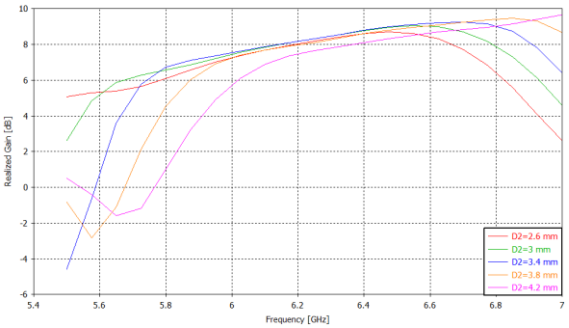

c)

Figure 2.50 Parametric analysis for D_2 parameter with Rogers 5870 substrate – a) Reflection coefficient, b) Axial ratio, c) Realized gain

From the graphs, a similar effect of the critical parameters of the antenna, analyzed previously with Arlon CuClad 217 substrate can be observed on the desired characteristics for optimization in this model with Rogers 5870 substrate, shown in Table 2.3. Therefore, these same parameters will be considered to determine a compromise for a high antenna performance.

2.4.3 Particle swarm optimization

Figure 2.51 a) shows the value ranges of the critical parameters where the antenna showed a proper efficiency in terms of S_{11}, axial ratio and gain of the new model with Rogers 5870 substrate. Figure 2.51 b) defines the parameters accordingly to the desired characteristics, in this step the same configuration as with Arlon Cuclad 217 substrate was applied. Figure 2.51 c) shows the values of the optimized parameters and the solver information. In order to attain a high accuracy in the optimization procedure of this model a higher number of evaluations was used than with the first model, with a total of 226 solver runs performed.

	Parameter	Min	Max
☒	D1	0.5	0.7
☒	D2	3	3.4
☐	phi1	13.5	16.5
☐	phi2	27.54	33.66
☐	phi3	9.9	12.1
☐	phi4	36	44
☐	phi5	5.4	6.6
☒	R5	12.9	13.1
☒	R6	6.2	6.4
☐	Rg	37.17	45.43
☐	ri	0.54	0.66
☐	ro	1.809	2.211
☒	S1	0.3	0.5
☐	S2	1.53	1.87
☒	S3	0.15	0.45
☐	S4	0.315	0.385
☐	t	0.0153	0.0187
☐	ts	2.862	3.498

a)

	ID	Type	Operator	Target	Range	Weight
☒	0	1DC: .\S-Parameters\S1,1	min	-120	6...6.5	1.0
☒	1	TBPP 1D: Axial Ratio	=	0	5.5...7	1.0
☒	2	TBPP 1D: Realized Gain	=	12	5.5...7	1.0

b)

```
Algorithm: Particle Swarm Optimization
226 of maximal 226 solver runs done

Number of evaluations: 226
                (solver: 226)
First goal function value   = 118.68148843
Best goal function value    = 115.773580177
Last goal function value    = 115.773580177

Best parameters so far:

 D1 = 0.676856
 D2 = 3.22457
 R5 = 13.0988
 R6 = 6.37199
 S1 = 0.496869
 S3 = 0.280819
```

c)

Figure 2.51 Particle swarm optimization with Rogers 5870 substrate – a) Critical parameters, b) Goals definition, c) Optimized parameters results.

Figure 2.52 shows the optimized characteristics of the antenna. In Figure 2.52 a) the reflection coefficient, the axial ratio and the realized gain are presented. It can be observed that the S11 parameter exhibits a good tuning the center of the operating band for both resonant frequencies. The lower resonant frequency at 5.98 GHz is -26.1 dB whereas the higher frequency at 6.75 GHz is -25.9 dB. The impedance bandwidth is 21.6% for |S11| < -10 dB from 5.58 GHz to 6.93 GHz. The axial ratio and realized gain are shown in Figure 2.52 b) The obtained axial ratio bandwidth is equal to 16.7% for AR < 3 from 5.81 GHz to 6.87 GHz. The minimum AR equal to 0.4 dB is obtained at 6 GHz. Moreover, the realized gain of the antenna is equal to 8.8 dB at 6.7 GHz. Both parameters were analyzed in the main lobe direction with an elevation θ =23°.

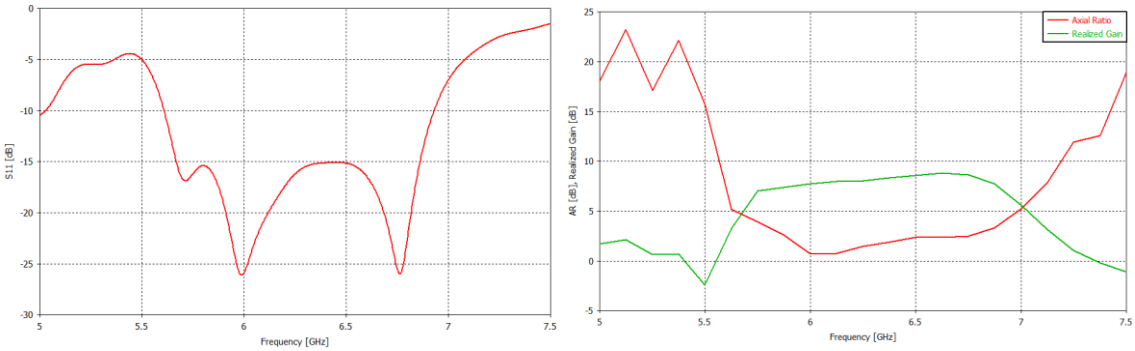

a) b)

Figure 2.52 Optimized characteristics with Rogers 5870 substrate – a) Reflection coefficient b) Axial ratio and realized gain.

Optimized directivity patterns in the H and E planes at 5.9 GHz, 6.3 GHz and 6.7 GHz, respectively, are shown Figure 2.53. The maximum gain at 6.7 GHz in the main lobe direction is depicted. The obtained peak gain is equal to 8.97 dBi and the elevation angle θ is equal to 23°. The side lobe level is -11.8 dB

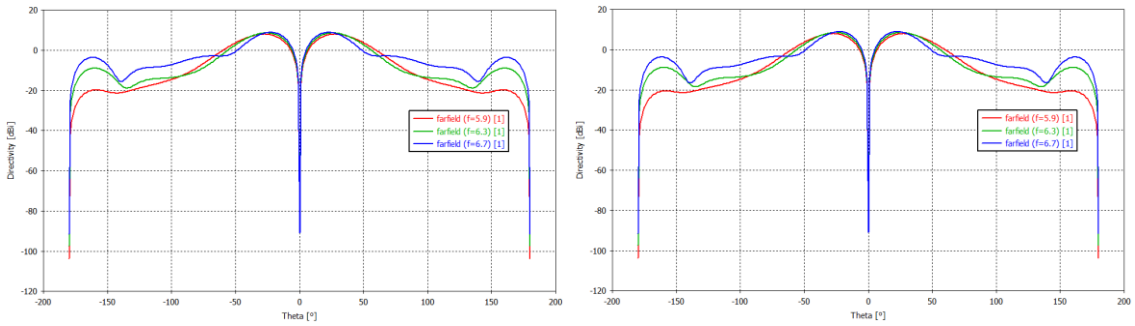

a) b)

Figure 2.53 Optimized directivity characteristics with Rogers 5870 substrate at 5.9 GHz, 6.3 GHz, 6.7 GHz in the – a) H-plane, b) E-plane.

Table 2.5 summarizes the results obtained with referral and optimized parameters of the antenna, in which again, as with Arlon CuClad 217 substrate, an enhancement by the compromise between the desired characteristics was achieved.

Table 2.5 Comparison of optimized and non-optimized characteristics with Rogers 5870 substrate.

	Frequency [GHz]	Impedance bandwidth [%]	AR bandwidth [%]	Peak gain [dBi]
Referral parameters	6.7	15.9	15.5	9.42
Optimized parameters	6.7	21.6	16.7	8.97

2.4.4 Recalculation for available fabrication

After the optimization procedure, the antenna was recalculated for the following reasons:

1. Available drills in the workshop for the elaboration of the vias were not identical to those used to obtain the parameter results in the optimization. Hence, for their elaboration, drills with the closest dimensions to the optimized model were used. These new dimensions of the vias were: D_1 = 0.6 mm (before 0.7), D_2 = 3.1 mm (before 3.4 mm). Table 2.6 shows these new values, together with the optimized and unchanged parameters for this final model for fabrication.
2. To achieve a solid and reliable implementation a circular shape for the substrate was not sculpted because of the sensitive vias around the antenna. Instead, a square shape of dimensions 9cmx9ccm was used.

Simulations of the antenna characteristics with both of these new features in the optimized model were performed in the Frequency Domain Solver with Adaptive Meshing. Figures 2.54 - 2.57 demonstrate that the overall antenna characteristics – impedance bandwidth, directivity patterns and axial ratio were not affected by these last modifications and keep their same tendencies shown in Section 2.4.3 after the optimization procedure.

Table 2.7 summarizes the simulated characteristics results of the final model to be fabricated to verify them experimentally in Section 2.6.

Table 2.6 Parameters of the final model of the antenna.

Parameter	Value	Parameter	Value
R_1	16	D_1	0.7
R_2	19.9	D_2	3.4
R_3	37.6	D_3	1.4
R_4	29.4	S_1	0.4
R_5	12.9	S_2	1.7
R_6	6.2	S_3	0.2
R_g	41.3	S_4	0.35
Φ_1	15	d_1	1.3
Φ_2	30.6	d_2	1.6
Φ_3	11	d_3	1.8
Φ_4	40	-	-

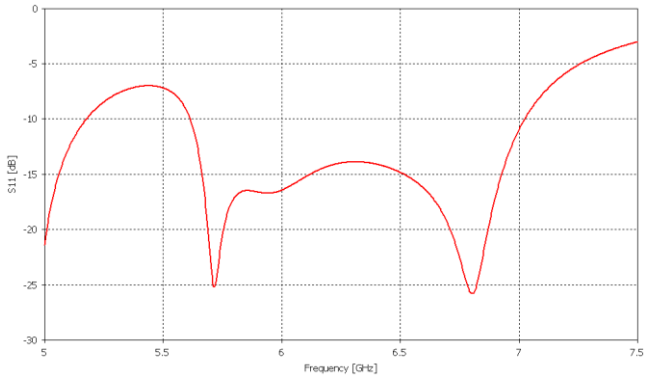

Figure 2.54 Reflection coefficient of final model with Rogers 5870 substrate.

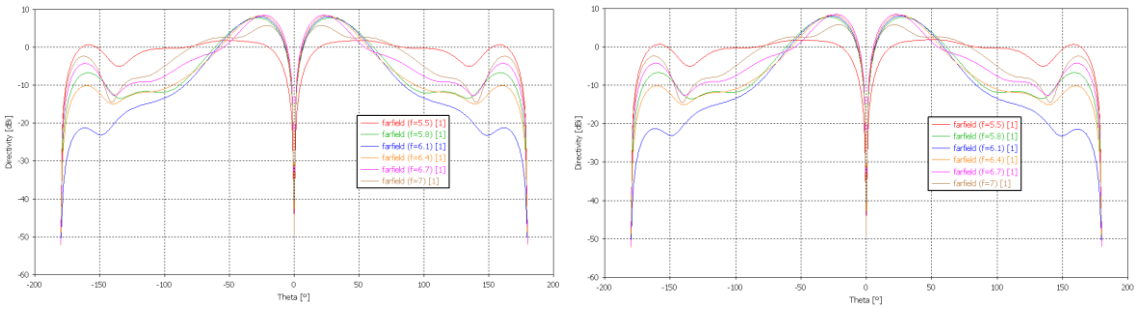

a) b)

Figure 2.55 Directivity characteristics of final model with Rogers 5870 substrate at 5.5 GHz, 5.8 GHz, 6.1 GHz, 6.4 GHz, 6.7 GHz, 7GHz – a) H-plane, b) E-plane.

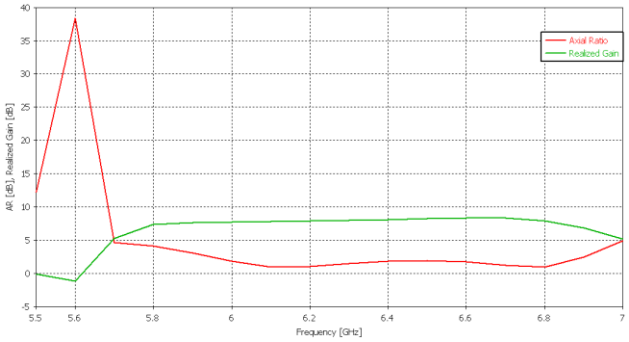

Figure 2.56 Axial ratio and realized gain of final model with Rogers 5870 substrate.

Table 2.7 Summary of simulated results of the final model for fabrication.

	Frequency [GHz]	Impedance bandwidth [%]	AR bandwidth [%]	Peak gain [dBi]
Simulated results	6.5	26.2	-	8.4

Characteristics were measured in the main lobe direction of the antenna with an elevation angle θ =24°.

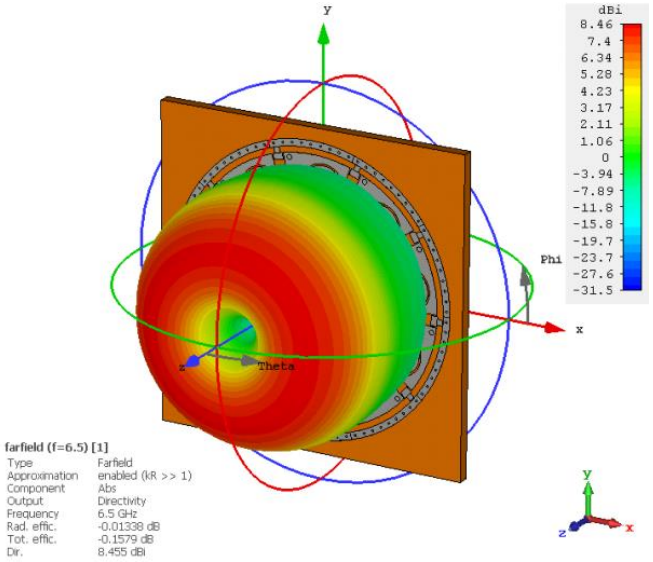

Figure 2.57 Radiation patterns in 3D view of the final model with Rogers 5870 substrate at 6.5 GHz.

Figures 2.58 (a-d) shows the current distribution on the surface of the final model for phases 0°, 60°, 120° and 180°, respectively.

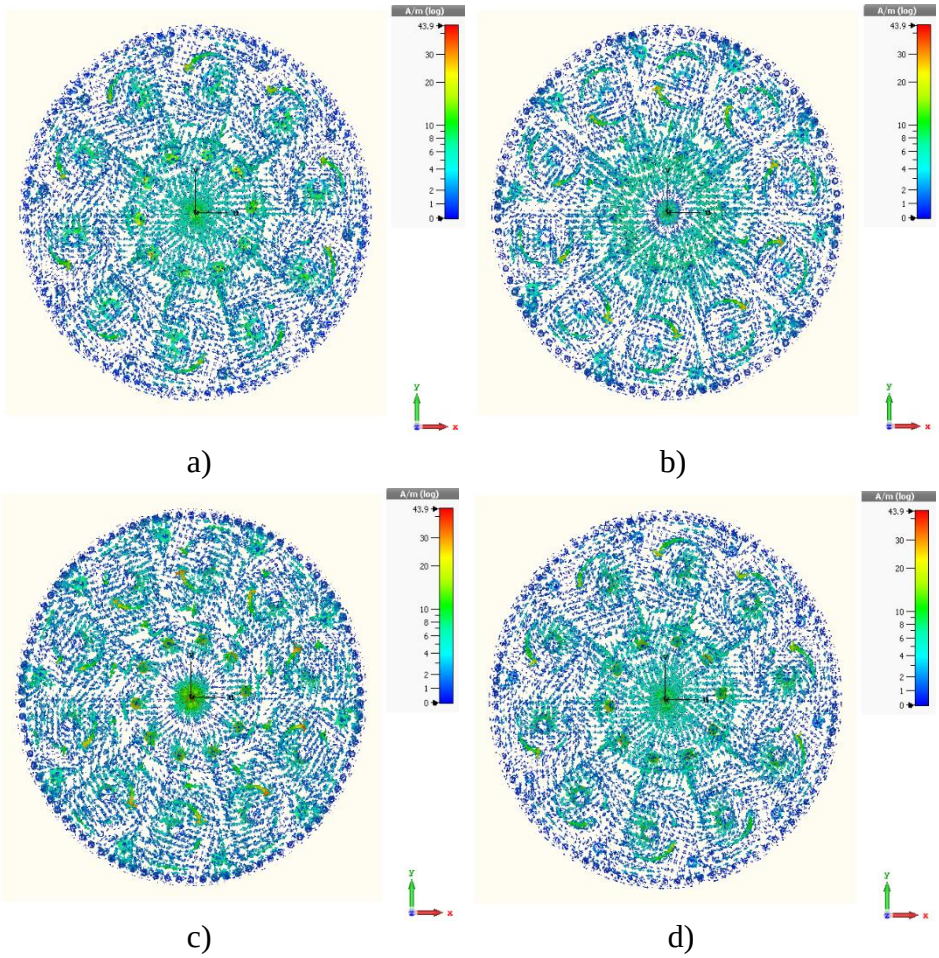

Figure 2.58 Current distribution on surface of the final model with Rogers 5870 substrate.

2.5 Fabrication

This section describes the fabrication process of the antenna, including the stages followed. Two stages were remarkable – the PCB process and the elaboration of the vias.

2.5.1 PCB process

The antenna was fabricated by the etching PCB process in the workshop of the Department of Radio Electronics of the FEEC BUT. The final design and drill document were exported from CST Microwave Studio 2018 to Gerber Gerbv 2.6A program in order to print the substrate and later drill the fabricated model.

As stated before, the model for fabrication was designed with Rogers 5870 substrate, which was provided by the DREL FEEC BUT. The principal advantage of this material was its good relative permittivity, which was suitable for a high performance in the desired 5.5 GHz - 7 GHz frequency band for the investigated antenna.

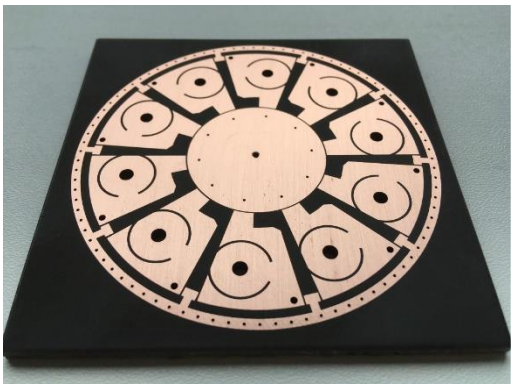

a)

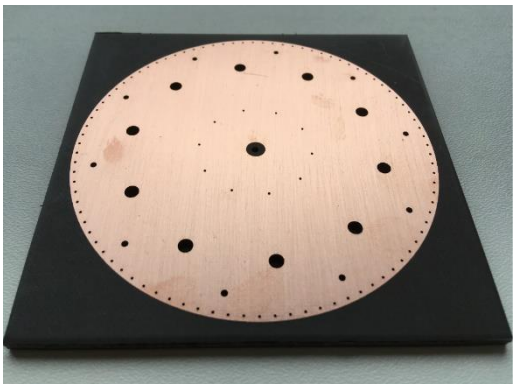

b)

Figure 2.59 Printed antenna board – a) Top side, b) Bottom side

2.5.2 Vias elaboration

After the fabricaton of the PCB previously designed and exported, the next step was the drilling of the vias for the antenna. The diameters of the machine tools which were used for drilling were 0.6 mm (for vias D_1 and edge vias around the antenna), 3.1 mm (for vias D_2) and 1.4 mm (for vias D_3).

The metallization of the holes was not able to be implemented in the workshop due to the wide thickness of the substrate and the Teflon material added to it. Hence, the approach to this step was to make the vias manually by soldering wires. This process was a standard soldering performed in the student laboratory. Wires used were:

- For the vias D_1 and edge vias around the antenna: wires of diameter 0.5 mm (Material: Brass).
- For the vias D_2*:* hollow tubular rivets of diameter 3.02 mm, height of 2.9 mm and cladding thickness of 0.4 mm. Rivets were elaborated manually as well. (Material: Brass)
- For the vias D_3*:* wires of diameter 1.37 mm (Material: Copper).

For the processing of vias D_1 and edge vias around the antenna, first the holes were embroiled with the wire and later soldered together.

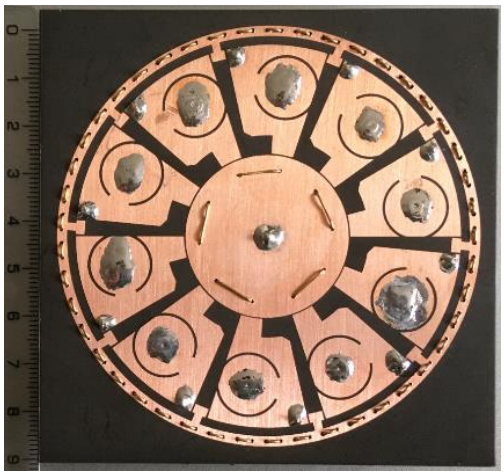

a)

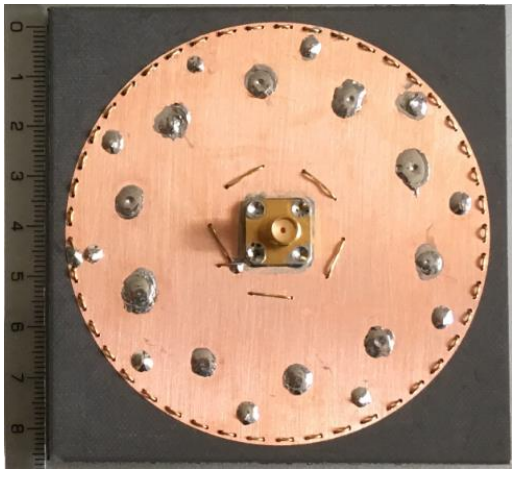

b)

Figure 2.60 Fabricated antenna with manual vias – a) Top side, b) Bottom side.

2.6 Measurements and experimental verification of simulated results

To experimentally verify the investigated antenna concept and its properties, the reflection coefficient, directivity characteristics, axial ratio and gain were measured.

2.6.1 Reflection coefficient (S_{11})

The reflection coefficient was measured in the laboratory of antennas of the FEEC BUT. For the measurement, Rohde&Schwarz ZVL vector network analyzer (9 KHz - 13.6 GHz) with calibration kit was used.

As can be observed from the comparison of both graphs, the measured results correspond to the simulation. The impedance bandwidth for $|S_{11}| < -10$ dB obtained is 26.2% from 5.44 GHz to 7.08 GHz, which covers a wider frequency band than the simulated. A small frequency shift in the lower resonant frequency is probably caused due to the extra layer of metallization in the via of the patch monopole (D_1) produced by the manual soldering. As reported in Table 2.3 after parametric studies, this is a critical parameter which has a bigger effect on the lower resonant frequency.

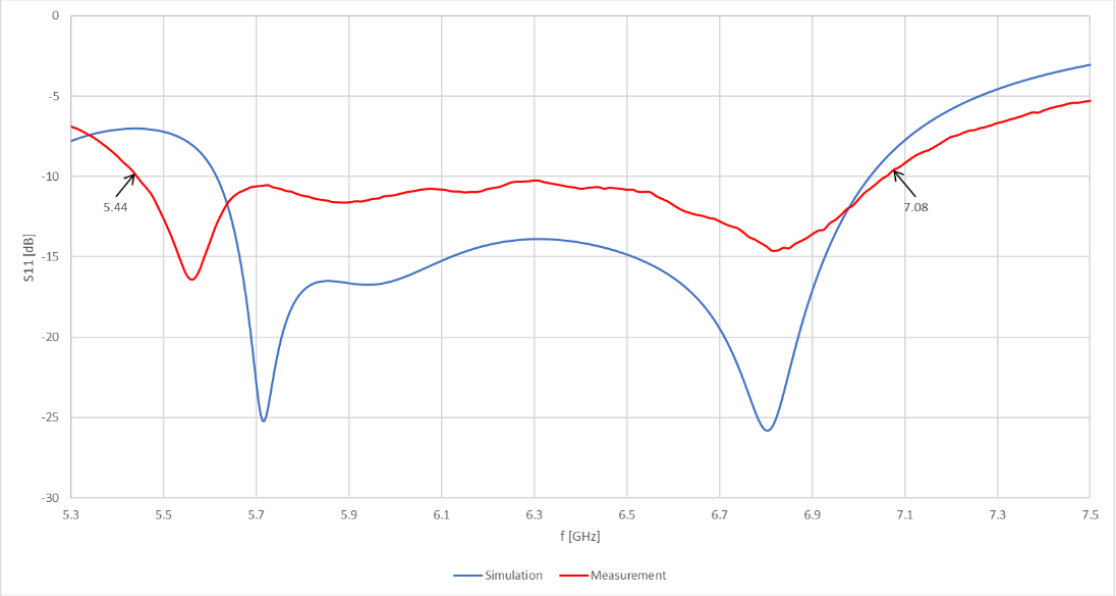

Figure 2.61 Measured and simulated reflection coefficient of the antenna.

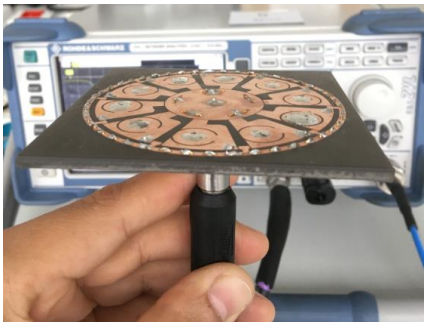

Figure 2.62 Measurement of the reflection coefficient.

2.6.2 Directivity characteristics

The directivity characteristics, the axial ratio, and the gain were measured in the anechoic chamber of the FEEC BUT. Directivity characteristics were measured in the far field in a θ range from -135° to 135° for RCHP. As can be observed in the comparison graphs, the measured results in both planes correspond to the results obtained in the simulations, which proves a correct performance of the fabricated antenna. The results at all frequencies are almost identical, except for slight frequency shifts at 5.5 GHz. This may be caused by many factors, such as non-ideal etching of the antenna model on the substrate and human error in the soldering of sensitive vias, which can affect directly the directivity characteristics.

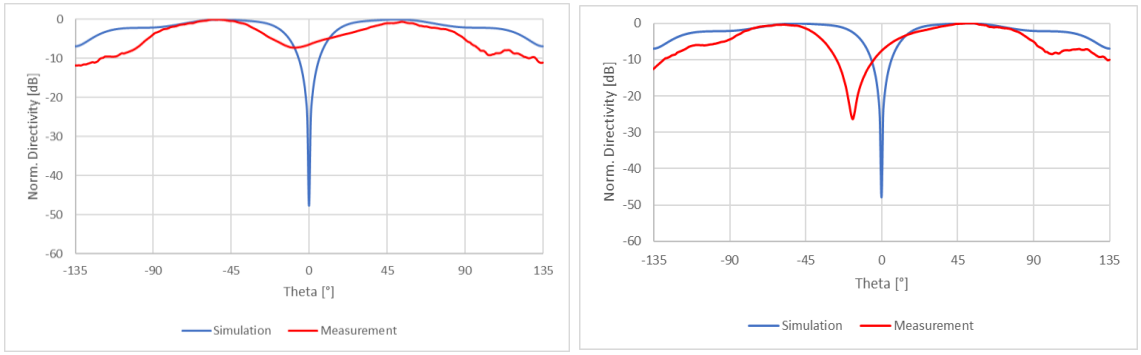

a) b)

Figure 2.63 Measured and simulated directivity at 5.5 GHz – a) H-plane, b) E-plane.

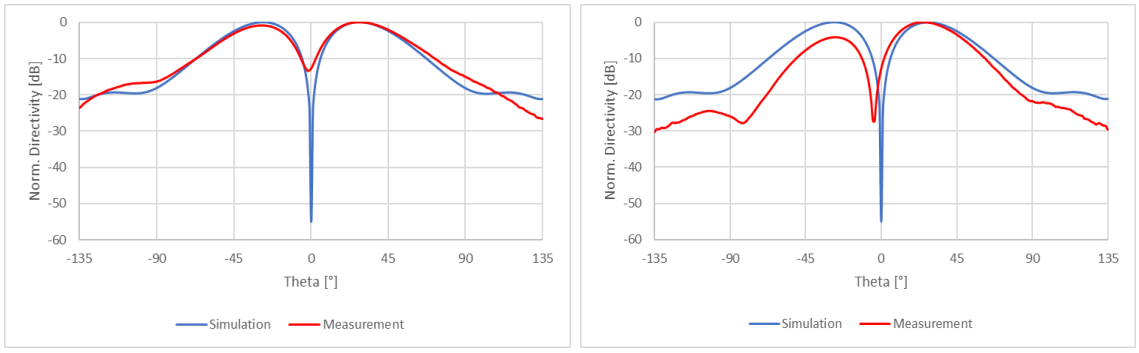

a) b)

Figure 2.64 Measured and simulated directivity at 5.8 GHz – a) H-plane, b) E-plane.

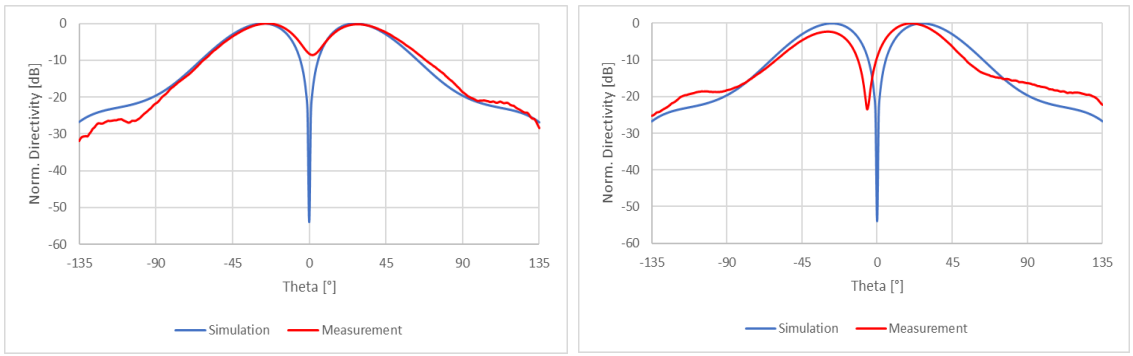

a) b)

Figure 2.65 Measured and simulated directivity at 6.1 GHz – a) H-plane, b) E-plane.

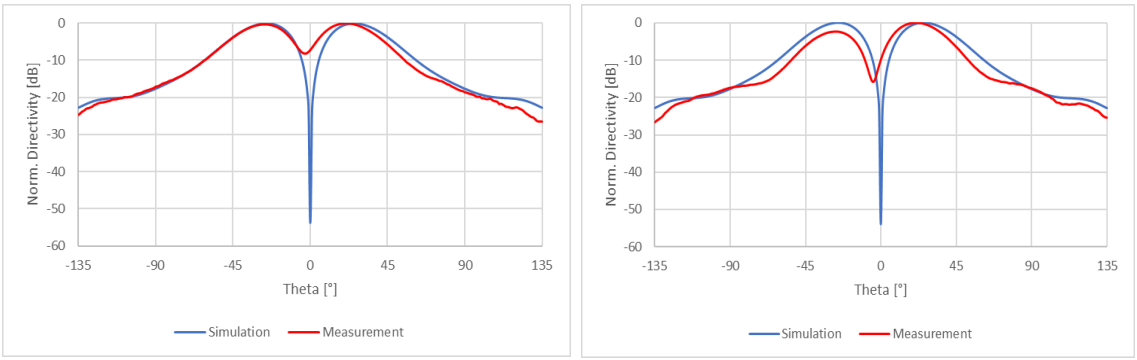

a) b)

Figure 2.67 Measured and simulated directivity at 6.4 GHz – a) H-plane, b) E-plane.

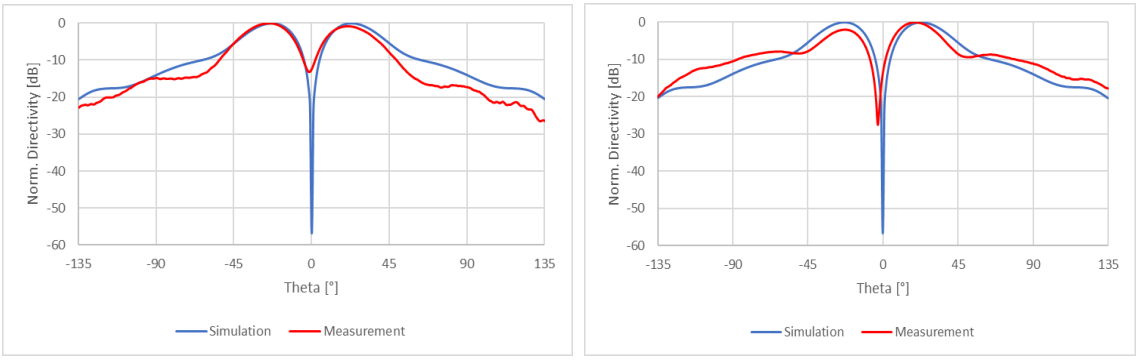

a) b)

Figure 2.66 Measured and simulated directivity at 6.7 GHz – a) H-plane, b) E-plane.

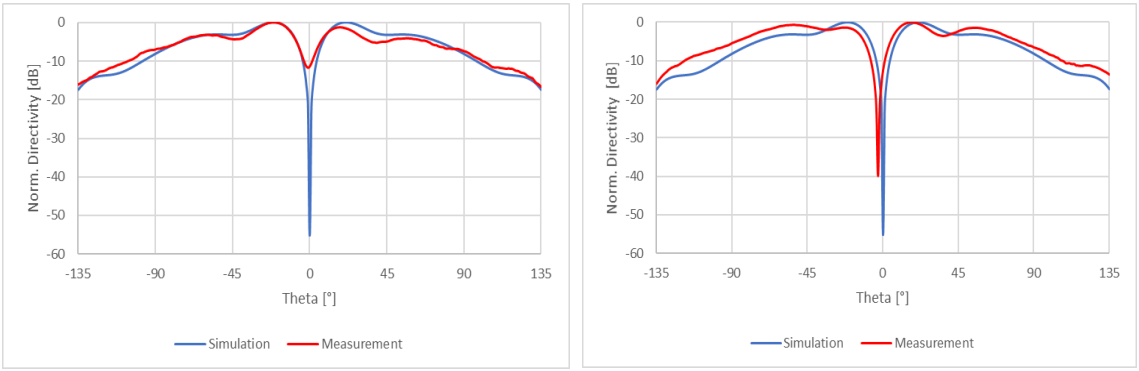

a) b)

Figure 2.68 Measured and simulated directivity at 7 GHz – a) H-plane, b) E-plane.

2.6.3 Axial ratio (AR)

The axial ratio of the antenna was measured in the main lobe direction of the antenna with an elevation angle θ =24°, previously depicted in simulated results of the fabricated model in Table 2.7. It can be observed from the measurement in the frequency range of the axial ratio that again this parameter shows a good agreement with the simulated results. However, the axial ratio does not drop to the simulated values around at the frequency of 6.15 GHz, but increases its level for approximately 150 MHz and then goes down again to keep a smooth curve accordingly to the simulation. This phenomenon may be caused by the non-ideal placement of metallization during the soldering of the shorting vias, inserted manually by wiring which introduced inaccuracy into the antenna structure. According to the study of the antenna mechanism, the shorting vias play a crucial role, together with size parameters of the stubs, for axial ratio and high gain performance.

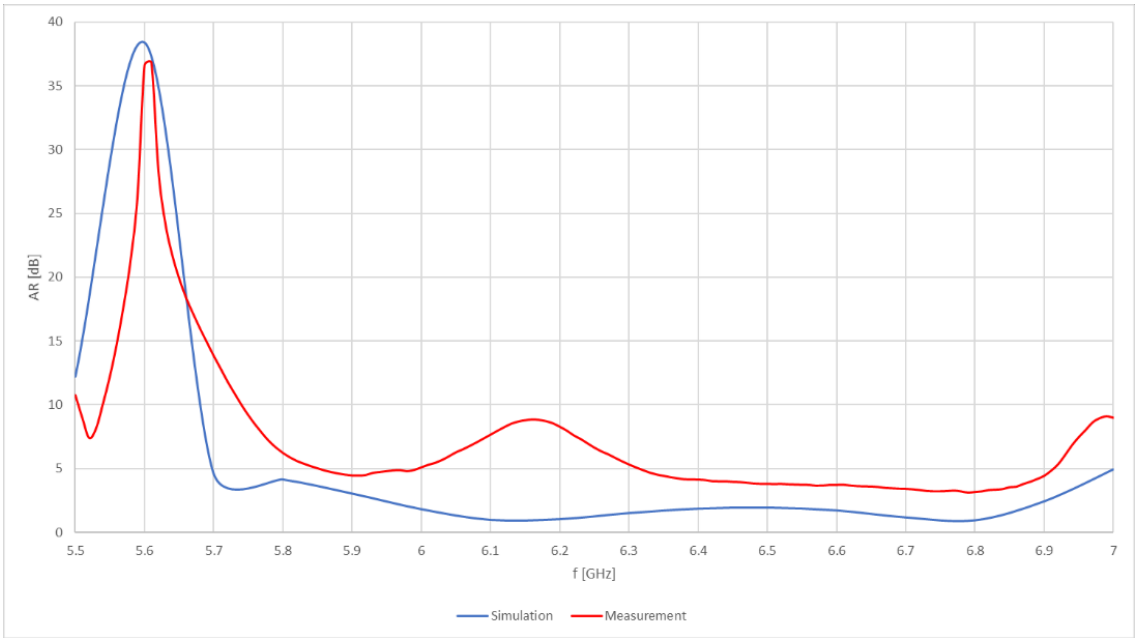

Figure 2.69 Measured and simulated axial ratio of the antenna.

2.6.4 Gain

Similarly, as the measurement of the axial ratio, the gain of the antenna was measured in the main lobe direction with an elevation angle θ =24° at 6.5 GHz, where the simulation reached a maximum gain of 8.4 dBi. The measured gain obtained at this frequency was 7.7 dBi, which can be considered as a solid result, despite of the fact, that sensitive parts in the model such as the vias, were elaborate manually which may be caused small loses in the inserted layers of soldering into the antenna structure. In addition to this, the margin of error of the measurement in the anechoic chamber nearly 0.3 - 0.4 dB can be also considered a probable cause.

3 CONCLUSION

This bachelor's thesis presented the design of a novel type of wideband low-profile circular array antenna with circular polarization and high gain, which was proposed in the primary literature. The main objectives of this design were to optimize the antenna in terms of the following characteristics: impedance bandwidth, axial ratio and directivity characteristics for a 5.5 - 7 GHz frequency band. In order to experimentally verify its properties, the investigated antenna had to be fabricated and measured. This bachelor's thesis is divided in two principal parts. The first part discussed fundamentals about microstrip and slot antennas, their essential characteristics and parameters, feeding, substrate integrated waveguide cavity resonator and planar circular array to subsequently present the design concept and the operating mechanism of the investigated antenna. The second part presented the design and realization approach to achieve the proposed antenna. The following 7 sections are remarkable in this part. The first Section 2.1 explained the method, steps and considerations performed for the numerical design and optimization procedure in the full-wave program CST Microwave Studio. Sections 2.2 - 2.4 focused on simulations for three numerical designs with different dielectric substrates – Taconic TLX, Arlon CuClad 217, and Rogers 5870. In addition to this, the optimization procedure of the antenna for both Arlon CuClad 217, and Rogers 5870 dielectric substrates was achieved and explained in detail. Sections 2.5 and 2.6 described the fabrication process and experimental verification by a comparison of measured and simulated results of the antenna. Finally, Section 2.7 showed a comparison of performance of the present work with other studies.

The investigated antenna was designed, optimized and fabricated on Rogers 5870 substrate. Despite the fact, that the most sensitive elements for the operation of the antenna, such as the vias, were create manually, the antenna exhibited overall a good performance, according to the measured results. The impedance bandwidth obtained was 26.2% from 5.44 GHz to 7.08 GHz presenting a wider impedance bandwidth than the simulation and covering frequency bands where the antenna could be used for various applications. The directivity characteristics obtained had good agreement with simulations. The axial ratio also exhibited a corresponding behavior to the simulation, except at frequency 6.15 GHz, where its level increased for approximately 150 MHz and then went down again following a smooth curve pattern which corresponds to the simulation. The cause was probably the inaccuracy added to the structure by manual soldering of the shorting vias in the antenna, which play a key role for axial ratio and high gain performance in its mechanism. In addition to this, the reached gain of the antenna in the main lobe direction with an elevation angle θ =24°.

In view of the above discussion, all the points of the assignment in this bachelor's thesis were fulfilled.

BIBLIOGRAPHY

[1] XU, H., ZHOU, J., WU, Q., YU, Z., HONG, W. *Wideband low-profile SIW cavity-backed circularly polarized antenna with high-gain and conical-beam radiation*. IEEE Transactions on Antennas and Propagation, 2018, vol. 66, no. 3, p. 1179-1188.

[2] BALANIS, C. A. *Antenna Theory: Analysis and Design*. 3rd Edition. Hoboken: J. Wiley & Sons, 2005. ISBN 0-471-66782-X.

[3] ZBITOU, J., ERRKIK, A. *Emerging Innovations in Microwave and Antenna Engineering*. Advances in Computer and Electrical Engineering (ACEE) Book Series. IGI Global, 2018. ISBN 1-522-57539-1.

[4] BHARTIA, P., BAHL, I., GARG, R., ITTIPIBOON, A. *Microstrip Antenna Design Handbook*. Norwood: Artech House, 2001. ISBN 0-89006-513-6.

[5] RAIDA, Z., et al. *Multimedia textbook: Electromagnetic waves, Microwaves technique* [online]. Brno: FEEC BUT Brno, 2010 [cit. 2018-11-10]. Available from URL: <http://www.urel.feec.vutbr.cz/~raida/multimedia/index.php>.

[6] MILLIGAN, Thomas A. *Modern Antenna Design*. 2nd edition. Hoboken: J. Wiley & Sons, 2005. ISBN 0-471-45776-0.

[7] CHEN, Z., CHIA, M. *Broadband Planar Antennas: Design and Applications*. J. Wiley & Sons, 2006. ISBN: 0-470-87174-1.

[8] AWIDA, M.H., FATHY, A.E. *Design guidelines of substrate-integrated cavity backed patch antennas*. IET Microwaves, Antennas & Propagation, 2012, vol. 6, no. 2, p. 151-157. ISSN 1751-8725.

[9] MIKULÁŠEK, T. *Microstrip patch antennas fed by substrate integrated waveguide*. Brno: Brno University of Technology, Faculty of Electrical Engineering and Communication. Department of Radio Electronics, 2013. pp. 87. Doctoral thesis. Supervisor: Ing. Jaroslav Láčík, Ph.D.

[10] LÁČÍK, J. *Mikrovlná technika: přednášky*. Brno: Brno University of Technology, Faculty of Electrical Engineering and Communication. Department of Radio Electronics.

[11] CST Studio Suite 2018 – User's brochure [online]. 2017 [cit. 2018-11-10]. Available from URL: <https://www.cst.com/products/csts2>.

[12] Coaxial Cable Impedance Calculator [online]. 2015 [cit. 2018-11-10]. Available from URL: <https://www.everythingrf.com/rf-calculators/coaxial-cable-calculator >.

[13] Slot Antennas. BEVELACQUA, Pete. The Antenna Theory Website [online]. 2010 [cit. 2012-04-15]. Available from URL: < http://www.antenna-theory.com/antennas/aperture/slot.php>

[14] Krairiksh, M., Phongcharoenpanich, c., Meksamoot, K., Takada, J. Characteristics of a circularly polarized conical beam spherical slot array antenna. IEICE Trans. Electronics, vol. E82-C, no.7, pp.1242-1247, July 1999.

[15] XU, H., ZHOU, J., YU, Z., ZHOU, K. *Low-profile circularly polarised patch antenna with high gain and conical beam*. IET Microwaves, Antennas and Propagation, 2018, Vol. 12 Iss. 7, pp. 1191-1195.

INDEX OF SYMBOLS, QUANTITIES AND ABBREVIATIONS

f	Frequency.
f_{max}	Maximum frequency.
f_{min}	Minimum frequency.
Q	Quality factor.
Z_0	Characteristic impedance.
Z_A	Antenna impedance.
ε_r	Relative permittivity.
ρ	Voltage reflection coefficient.
S_{11}	Reflection coefficient at the input.
λ	Wavelength.
E	Electrical field vector.
H^*	Complex conjugate vector of the magnetic field phasor.
$D\ (\varphi, \vartheta)$	Directivity factor.
U	Radiation intensity.
G_{abs}	Absolute gain.
CP	Circular polarization.
CST	Computer simulation technology.
PCB	Printed circuit board.
MIC	Microwave integrated circuit.
DBS	Direct broadcasting satellite.
VSWR	Voltage standing wave ratio.
BW	Bandwidth.
IBW	Impedance bandwidth.
GBW	Gain bandwidth.
ARBW	Axial ratio bandwidth.
RHCP	Right hand circular polarization.
LHCP	Left hand circular polarization.
AR	Axial ratio.
SIW	Substrate integrated waveguide.

A ANTENNA DESIGN

A.1 Gerber layout – Top side

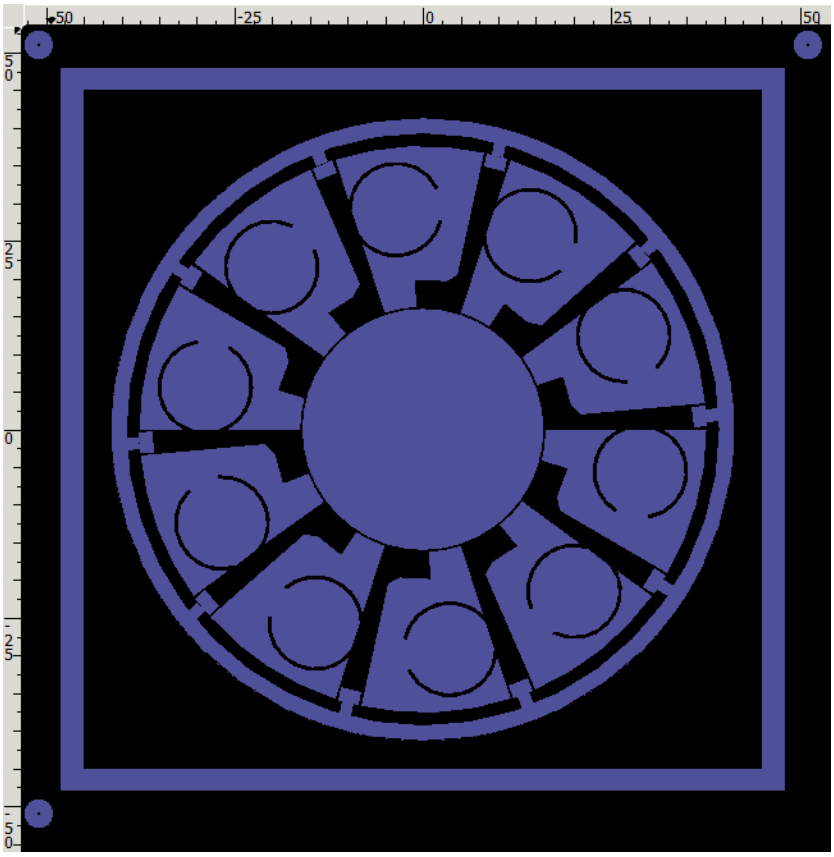

Dimensions of board 90 x 90 [mm], scale M1:1

A.2 Gerber layout – Bottom side